NASA-CR-203303

Computational Aeroservoelastic Analysis with an Euler-Based Unsteady Flow Solver

NASA-Ames University Consortium Cooperative Agreement No. NCC2-5105

Final Research Summary

for the period: 1 November 1994 - 31 January 1997

NASA Technical Monitor:
Dr. Kajal K. Gupta
NASA Dryden Flight Research Center
Edwards, CA

Principal Investigator:
Dr. Andrew S. Arena, Jr.
School of Mechanical and Aerospace Engineering
Oklahoma State University
Stillwater, OK

take weeks to run. For this reason, an alternative approach for solving time-varying boundary conditions called the transpiration boundary condition, has been adopted.

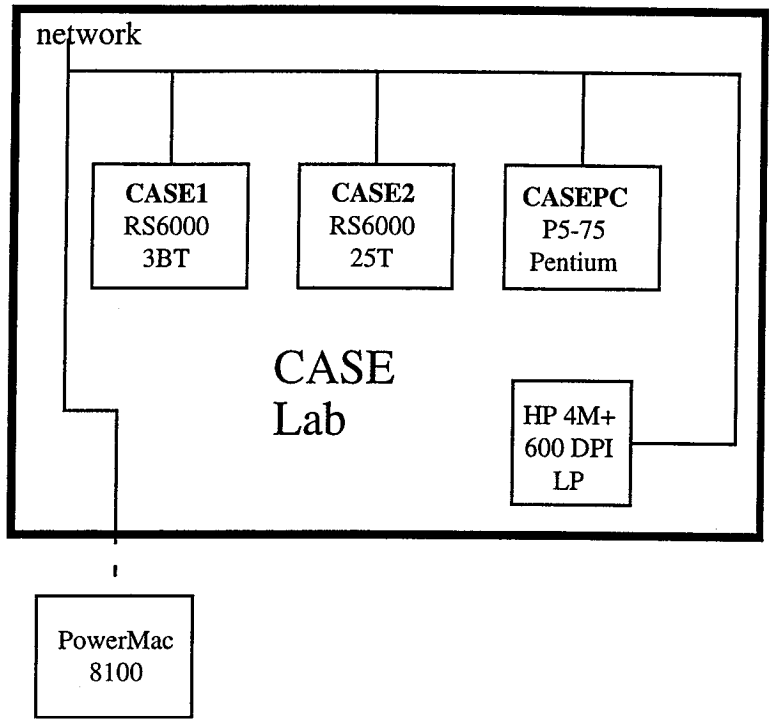

Figure I CASE Lab Hardware

The transpiration boundary condition requires no alteration of the initial discretized computational domain, thus saving the large amount of time required for rediscretization. The method alters only the normal vector and unsteady velocity boundary condition at each node on the surface of the body under investigation. The approach has a limitation however in that as surface deflections become larger, the validity of the transpiration assumption is reduced. In the present investigation outlined in section I, the transpiration boundary condition has been tested over a wide Mach number range (from subsonic through supersonic) for a variety of configurations. Results indicate that even for relatively large structural deformations, the transpiration boundary condition remains a very effective method for simulating changing aeroelastic boundary conditions. This makes the method particularly useful for defining local aeroelastic instabilities over a wide rang of operating conditions for geometries of practical interest.

3. Alternative Supersonic Aerodynamic Prediction Methodology

An enhancement to the STARS integrated analysis tool has been developed in order to improve the practicality of time-marched supersonic aeroelastic solutions in an operational environment. A significant drawback of the time-marching approach is the computation time required to complete the search. The use of time-marching solutions to the Euler equations on three-dimensional configurations of practical interest requires significant computational time in order to insure time accuracy. The goal of the present study has been to enhance the practicality of the time-marching supersonic aeroelastic analysis through a synergistic combination of aerodynamic modeling techniques and CFD in order to significantly reduce the computation time required.

A variety of techniques were investigated to accomplish the task, and two methodologies have been implemented into the STARS code. Details of the methods may be found in Section II. In the first approach, a combination of piston theory with a modified Newtonian theory are implemented in a manner completely independent from the Euler Solver. In the latter approach,

the speed of the method is retained, with an ability to capture nonlinearities in the flow through a combination with the available steady Euler solution. A supersonic steady-state solution for the three-dimensional flowfield is obtained with the use of the finite-element Euler methodology. The flow variables obtained in the steady solution are saved, and treated as a mean flow condition which becomes the starting point for the aeroelastic simulation. The unsteady aerodynamic pressure is assumed to be a small perturbation about the mean flow at every surface node point through a local application of the isentropic wave equation. In this manner, nonlinearities due to 3-dimensional effects such as shock interactions are accounted for in the mean flow, and unsteady effects are treated as local perturbations. The unsteady generalized forces are obtained via integration at each time step, and the solution is marched in time. The process is repeated over the entire parameter space until a flutter boundary is defined.

Due to the speed of the method, flutter boundary estimation may be approached through the use of a search procedure while time marching, as opposed to polynomial interpolation of damping values. The critical parameters obtained through the boundary estimate procedure are then used in the time marching aeroelastic solution using the finite element Euler methodology. Results indicate that estimates obtained by proceeding in this manner are sufficiently close enough to the boundary obtained by the Euler method (over the range of validity), that the CFD solution may then be used for refinement which requires significantly fewer transient calculations.

Results obtained to date indicate that the combination of aerodynamic modeling with the CFD methodology can enhance the practicality of the use of time-marching CFD for supersonic aeroelastic calculations in an operational environment. For the configurations tested, it was shown that the time required to predict flutter by time marching CFD can be significantly reduced by first obtaining an accurate estimate using modeling techniques. Present experience indicates significant savings in identifying critical flight conditions for aircraft-type configurations. An added advantage of the presented approach is that the same grid may be used for the steady CFD solution, the perturbation model, and the time marching CFD solution. In addition, the method used can be easily implemented in any CFD algorithm capable of simulating supersonic flowfields with a relatively minimal increase in code size and complexity.

SECTION I

TRANSPIRATION BOUNDARY CONDITION STUDY

TABLE OF CONTENTS

CHAPTER 1

INTRODUCTION

1.1. Background

Ever increasing technological advancements have lead to the development of aircraft that operate at greater and greater velocities. Today, aircraft that are designed and manufactured to perform near and above sonic speeds are much more common. For example, it is typical for aircraft, from military fighter planes to modern airliners, to have cruise speeds in the transonic range. In the design and performance analysis of these vehicles, it is important to study their aeroelastic characteristics. Even for vehicles traveling at subsonic speeds, the flow can cause a body deformation in the structure, which in turn will affect the flow solution. The coupling between fluid and structural forces can induce unstable oscillations. Therefore, it is important to accurately predict a vehicle's flutter boundaries, since inaccurate predictions could result in vehicle failure.

Often in modern three-dimensional aeroelastic analysis, a flow solver is employed in conjunction with a structural solver. The solutions of the flow field and the surface oscillation are performed simultaneously. Many flow solvers used today employ a grid

and the surrounding flowfield. Movement of the body under investigation due to the surface loads must be accounted for. This requires that either the surface grid be modified to match the body deflection, or that the deflection be simulated by some means. One possibility for simulating the deflection is to modify the surface normals at their original locations. Thus, to the flow field, the surface appears to have an altered form. This concept is known as the transpiration boundary condition and is the focus of this study.

1.2. Problem Statement

In unsteady aeroelastic analysis, the position and orientation of the surface under investigation are a function of time. In order for the solution to be determined accurately, the surface deformation must be represented. The most direct representation would appear to be regenerating the computational grid. However, in a time stepping approach, this would require that the grid be regenerated at each time step, since the surface will change with every time step. Using this procedure with present computer capabilities, a solution for a single set of parameters using grid regeneration could be on the order of weeks.

The present study uses an integrated computer code called STARS (STructural Analysis RoutineS) that is capable of performing the steady and unsteady fluid and structural analysis of flight vehicles that are required for determining flutter boundaries. The Euler based flow solver is a recent addition to the code and is capable of simulating

three-dimensional compressible inviscid flows. It uses finite element techniques with unstructured adapted meshes of tetrahedral elements. Flow solutions using this code are performed in a time-marching fashion. Thus, in unsteady aeroelastic applications, the surface deformation must be represented at each time step. This is accomplished using the transpiration boundary condition in which the original computational domain remains unaltered. The surface deflections are simulated by applying the deflected body normals at the undeflected body location, thus reducing the time required for determining flutter boundaries.

1.3. Motivation for the Study

In any field of study it is important to search for ways of improving solution characteristics, whether it be solution accuracy, expediency, or cost efficiency. A coupled fluid-structure time marching solution can be highly time consuming. For example, on present high-speed workstations, the calculation of a single fluid-structure transient on a three-dimensional aircraft configuration using the Euler equations may require over 100 cpu hours. Therefore, it is highly desirable to develop means of reducing the required computational time while maintaining solution accuracy. Advancements in computer technology are continually assisting in this task. However, faster computers are generally more expensive, so what is gained in speed may be lost in cost. By introducing

new concepts in lieu of or in conjunction with existing methods, vast improvements in solution characteristics can often be made without significantly adverse effects.

Considering the time required to generate a single domain mesh for a flow solution, it seems highly impractical to rediscretize the computational domain at each time step. One alternative to this rediscretization was presented by Batina (1989) where he used a dynamic mesh algorithm that models a triangulated mesh as a spring network. Each edge of each triangle in the mesh is modeled by a spring whose stiffness for any edge i-j is inversely proportional to the length of the edge.

In this algorithm, the grid points on the outer boundary of the mesh are fixed and a predictor-corrector procedure that iteratively solves the static equilibrium equations in the x- and y-directions at each time step is used to determine the displacements δ_{xi} and δ_{yi} at each interior node i. The method predicts displacements according to

$$\tilde{\delta}_{x_i} = 2\delta^{n}_{x_i} - \delta^{n-1}_{x_i}$$

$$\tilde{\delta}_{y_i} = 2\delta^{n}_{y_i} - \delta^{n-1}_{y_i}$$

It then corrects the displacements using several Jacobi iterations of the static equilibrium equations using

$$\delta^{n+1}_{x_i} = \frac{\sum k_m \tilde{\delta}_{x_m}}{\sum k_m}$$

$$\delta_{y_i}^{n+1} = \frac{\sum k_m \tilde{\delta}_{y_m}}{\sum k_m}$$

where k_m is the spring stiffness, and the summations are over all edges of the triangles that have node i as an endpoint. Finally, the new nodal coordinates are given by

$$x_i^{n+1} = x_i^n + \delta_{x_i}^{n+1}$$

$$y_i^{n+1} = y_i^n + \delta_{y_i}^{n+1}$$

This algorithm was found to produce good results when used in unsteady pitching and plunging studies, and also in the prediction of flutter boundaries. However, it is necessary to perform the displacement calculations at each node for every time step in both coordinate directions. Additional computations will be required if the algorithm is extended to three-dimensions.

This number of calculations can be significantly reduced if the surface deflection can be simulated without having to alter the existing grid. One way to simulate body deflection is to apply a transpiration boundary condition at the surface. This is essentially done by rotating the body normals so that the new normals are in the same directions they would be in if the body had actually deflected. Thus the original body grid remains unaffected throughout the flutter investigation.

Transpiration has been used effectively in simulating surface deformations in full potential solutions and steady and unsteady rigid-body applications in Euler equations. It

is the purpose of this study to show the extent to which the transpiration boundary condition may be used in unsteady aeroelastic problems.

1.4. Rationale

When the transpiration boundary condition is employed, there is potential for great savings in time requirements. However, an expedient solution is useless if its accuracy is questionable. Therefore, showing the extent to which the transpiration boundary condition is valid will allow flutter investigations to be made much more quickly and with confidence in results when inside the transpiration limits.

1.5. Flutter Analysis

Pertaining to aerodynamics, flutter is the divergent oscillation of a surface resulting from a coupling between structural and fluid forces. The prediction of flutter boundaries has been the subject of a great deal of studies. Methods that have been used in many recent studies include full potential and Euler methods. Both methods have proven effective in many flutter investigations.

Full potential methods offer accurate solutions in a wide range of applications with relatively low computational costs. As with Euler methods, there is the assumption of

inviscid flow. However, since these methods use an approximation of the Euler equations, they require further assumptions. One assumption in the development of the full potential equation is irrotational flow, which in most cases is a reasonable solution. These equations also do not allow for entropy changes across shocks. Thus, the existence of shocks, even in subsonic flow, will introduce inaccuracy to the solution.

Euler methods produce a higher order, more accurate solution than the full potential methods. They are capable of accounting for viscous and entropy effects, therefore they can be used for studies of a much wider variety than the full potential methods, such as at high Mach numbers and with strong shocks. One drawback with these methods is that they are more computationally intensive. However, with ever increasing advancements in computer technology, these methods are becoming much more computationally affordable and widespread.

1.6. Literature Review

1.6.1. Transpiration Concept

In 1958, M. J. Lighthill presented four alternatives for the treatment of displacement thickness. One of these alternatives was termed "method of equivalent sources". The idea used in this method has today developed into what is known as transpiration. Rather than thickening an airfoil to account for the boundary layer, an

equivalent surface distribution of sources is used to "simulate" a thicker airfoil. This is done by modifying the normal velocity just outside the boundary layer to include additional outflow due to the boundary layer.

1.6.2. Transpiration in Full Potential Studies

One early study in which transpiration was used in conjunction with a flutter solution was performed by Sankar, Malone, & Tassa [1981]. The study was performed using a full potential method. Although not explicitly stated, transpiration was used in "simulating" the first order bending of an oscillating rectangular wing in subsonic flow. This was done by applying the zero normal velocity boundary condition for the deflected surface at the undeflected wing position. Computations were also performed by applying the boundary condition at the actual surface. The authors reported making both computations to ensure that the differences were small, however, results were only presented for the transpiration solutions.

Lift, moment, and phase results were presented for the transpiration computations at a Mach number of 0.24 and were compared to experiment and Kernel function solutions. It was concluded that the results compared reasonably well. It was noted that the simulated results more closely resembled the Kernel function than the experiment. This was attributed to neglecting viscous effects and the fact that the experiment used a

5% thick circular arc airfoil. Furthermore, it was concluded that the simulation accurately and reliably predicts unsteady subsonic potential flow.

This transpiration boundary condition was further used in a study of a fighter wing in transonic flow [Malone, Sankar, & Sotomayer, 1984]. The study incorporated transpiration with the full potential equations to estimate the 1st harmonic, real and imaginary components of unsteady surface pressures at eight different stations on an F-5 fighter wing. Computed and experimental results were presented for three transonic Mach numbers (0.8, 0.9, and 0.95). It was concluded for this study that the results correlated reasonably well. It was further concluded that this method could be used in studying flutter behavior of fighter type wings at transonic speeds.

Based on these validating results, Malone & Sankar [1985] used transpiration with full potential equations to study the unsteady pitching oscillation for the RAE wing-body model in transonic flow (Mach = 0.8). Unsteady surface pressure results were presented, however, no experimental data was available for comparison.

Then, in 1986, a study was performed exclusively to compare results from a full potential method using the exact boundary condition and the transpiration boundary condition [Sankar, Ruo, & Malone]. Results were presented for a NACA 64A006 airfoil with an oscillating trailing edge flap, a large aspect ratio wing in independent pitching and plunging, a plunging fighter wing, and a steady rectangular wing.

The NACA 64A006 results were computed at a freestream Mach number of 0.875. The results showed that pressure distributions were within plottable accuracy of one another, and that integrated loads were within 10% of each other. The first harmonic out

of phase component of the surface pressure distribution was also determined for the flap case and compared to experiment. Results for both exact and transpiration approaches and experimental data were found to be in close agreement, the only appreciable difference being near the sonic line.

The next configuration in the study was a large aspect ratio wing. Results were presented for three plunge velocities (corresponding to 1, 5, and 10 degrees steady angle of attack) at Mach = 0.77. At 1 degree, the results proved to be nearly identical. At the larger plunge values, the results were not as close but still very good (within 10%). Pitching results using the transpiration approach were also computed at Mach = 0.66 and compared to results from a vortex lattice method (for pitching rates of 1, 5, and 10 degrees/second). In each case, the transpiration prediction was larger than that of the vortex lattice method, the worst case being over 30%. However, the vortex lattice method does not consider airfoil thickness effects and therefore underpredicts the airloads.

Surface pressure distributions at four span locations were present for a Mach 0.95 fighter wing undergoing constant plunging motion (1.5 degrees effective plunge velocity). Transpiration and exact approaches were compared with experiment. Both approaches were found to closely match experiment, except for slightly smeared shocks predicted by transpiration. This was suspected to be due to the use of a somewhat coarser grid in the transpiration case.

The final study used transpiration to simulate steady viscous effects of a rectangular wing in transonic flow. The wing was analyzed at an angle of attack of 2.0 degrees and a Mach number of 0.8. Surface pressure distributions were calculated, with

and without viscous corrections, and compared with experiment. Solution accuracy showed improvement when transpiration was used for viscous corrections.

It was concluded from this study that for small amplitude motions, as in aeroelastic applications, the transpiration boundary condition provides accurate results. Furthermore, the authors cited a considerable savings in coding effort and memory requirements when using the transpiration boundary condition.

1.6.3. Transpiration in Euler Studies

The transpiration boundary condition was used with the unsteady Euler equations in a study of transonic flow past a fighter wing by Sankar, Malone, & Schuster [1987]. The pitch oscillation of the fighter wing was accounted for by changing the boundary condition and leaving the original surface unmodified. In-phase and out-of-phase components of the surface pressure distribution were calculated at four span locations and compared with experiment. The fighter wing Mach number was 0.8, and the pitching amplitude was 0.113 degrees at 40 Hz (zero mean angle of attack). Slightly higher suction levels were predicted by the Euler solver for the in-phase component near the leading edge. However, overall experimental and calculated results were found to be in very good agreement. It was concluded by the authors that the unsteady Euler solver with transpiration was robust enough and accurate enough to be used in aeroelastic studies.

Transpiration was again used in the unsteady Euler investigation of two pitching wings; a transonic (Mach 0.82) transport-type wing and a subsonic (Mach 0.7) rectangular wing [Ruo & Sankar, 1988]. The transport-type wing was the Lockheed-Air Force-NASA-NLR (LANN) wing. Its oscillating pitch amplitude was 0.6 degrees at a frequency of 24 Hz. The rectangular wing's oscillating pitch amplitude was 2 degrees at a frequency of 10 Hz.

In-phase and out-of-phase components of the surface pressures were presented for calculated and experimental results at four span locations for each wing. For the LANN wing, there are significant differences in results at some locations. However, according to the authors, the experimental data at many locations is not considered reliable for this wing. When the unreliable data is ignored, results for both components show good agreement. For the rectangular wing, calculated and experimental results agree everywhere except near the wing tip for the in-phase component, which may be due to viscous effects.

Midspan unsteady pressures were compared for both exact and transpiration methods. For the LANN wing, a steeper variation of the pressure near shock waves was predicted by transpiration, but away from shocks, the results were very similar. For the rectangular wing, almost identical results were predicted by both methods.

For this study, it was concluded that the overall agreement of results was good. However, the issue of which boundary condition was more favorable for small-amplitude motions was inconclusive.

More recently, a study was performed using transpiration with an Euler method to simulate control surface deflections [Raj & Harris, 1993]. The study included the trailing-edge flap deflections for a NACA 0012 airfoil and for an arrow-wing body configuration. Actual and simulated surface pressures were presented for the NACA 0012 airfoil with a 10 degree flap deflection at Mach numbers 0.6 and 0.9. For both Mach numbers, the transpiration method produced results that were in very good agreement with actual results.

The arrow-wing body configuration was analyzed using both a coarse and a fine grid, the fine grid having higher resolution around the wing. Simulated results were computed and compared with experimental data. Surface pressure distributions were presented at three span locations for 0, 4, and 8 degrees angle of attack with and without a flap deflection of 8.3 degrees. No experimental data was presented for the zero degree case with no flap deflection, but results for the fine and the coarse grids were in close agreement. Results from both grids matched well with experimental data for flap deflection at zero angle of attack.

Some noticeable differences between computed and experimental results can be seen for the outermost station in the 4-degree angle of attack case, while there is better agreement at the inner stations. However, these differences are most likely due to limitations of Euler equations, such as neglecting viscous effects, rather than transpiration. Also, the finer grid appears to produce data near the leading edge that is slightly closer to the experimental.

In the 8-degree angle of attack case, results for the innermost station are very close. Differences are seen at the middle station, but they are not a result of transpiration. The differences are a result of Euler computations producing attached flow where experimental data suggests flow separation at the leading edge. The outermost station results are not as good as the innermost, but results there are comparable.

Experimental and simulated lift and pitching-moment coefficients were also compared for the arrow-wing body case. Results were presented for 0, 8.3, and 17.7 degree trailing-edge flap deflections at Mach 0.85. For each flap deflection, the simulated lift and pitching moment results were in very close agreement.

From this study, the authors concluded that transpiration boundary condition was effective in estimating the changes in aerodynamic forces, moments and surface loading due to control-surface deflections, assuming that the Euler equations are capable of modeling the flow field. It was noted that transpiration was not suitable for simulating configurations that may produce geometric gaps.

1.7. Objectives of the Present Study

The STARS group, for which this study was performed, has recently added an unsteady Euler flow solver that uses transpiration to simulate surface deflections and deformations. The primary objective of this research is to employ this new code over a

wide Mach number range in the analysis of unsteady aeroelastic problems, and to document the extent to which the transpiration boundary condition is effective.

It is evident that the transpiration boundary condition can be used effectively to a large extent in applications of relatively small displacements. It is also apparent that this boundary condition can be an effective tool in aeroelastic investigations. However, it is important to be aware of what circumstances will cause the boundary condition to introduce appreciable inaccuracies. Therefore, this study will present the rationale for when and why the transpiration boundary condition will give inaccurate results and to perform investigations to support the rationale.

A secondary objective of this study is to determine how much influence grid resolution has on any given solution. This is a direct result of the primary objective because it is important to distinguish between inaccuracies due to transpiration and mere differences due to mesh sensitivity.

CHAPTER 2

METHODOLOGY

In this research effort, the transpiration concept was applied to various steady and unsteady cases. The preliminary results were obtain using a steady panel code that was modified to use transpiration for steady deflections. The majority of the results obtained from this study used an Euler based code that employs the transpiration boundary condition in steady and unsteady surface deflections and deformations. Computer codes were also developed in this study to produce actual surface deflections for use with the Euler code.

2.1. Transpiration Development

The idea of transpiration was first developed by Lighthill [1958] as a method of equivalent sources. Lighthill modified the normal velocity just outside the boundary layer of an airfoil through an equivalent surface distribution of sources to "simulate" a thicker airfoil. In this way, the effect of a boundary layer is present in the solution without

physical representation of a true boundary layer. Applied mathematically, the normal velocity w is

$$w = \int_0^z \frac{\partial w}{\partial z} dz = -\int_0^z \frac{\partial u}{\partial x} dz = -\frac{dU}{dx} z + \frac{\partial}{\partial x} \int_0^z (U - u) dz = -\frac{dU}{dx} z + \frac{d}{dx} \int_0^\infty (U - u) dz.$$

where z is the distance from the surface and u is the x component of velocity, which takes the value U just outside the boundary layer. The first term is the original, unmodified normal velocity. The second term represents the normal velocity contribution from the boundary layer. Thus, the flow field "sees" the effects of a boundary layer that is not physically present.

In this study, transpiration is applied as a boundary condition such that geometric changes and motions are simulated through surface transpiration. The unsteady boundary condition states that the velocity component normal to the body surface must equal the velocity of the body surface,

$$\mathbf{V} \cdot \mathbf{n} = \mathbf{V}_{body} \cdot \mathbf{n}$$

thus there can be no flow through the surface. With transpiration, this done by adding a velocity component normal to the tangential velocity so that the resultant velocity is at some angle to the original surface, as shown in Figure 2.1.

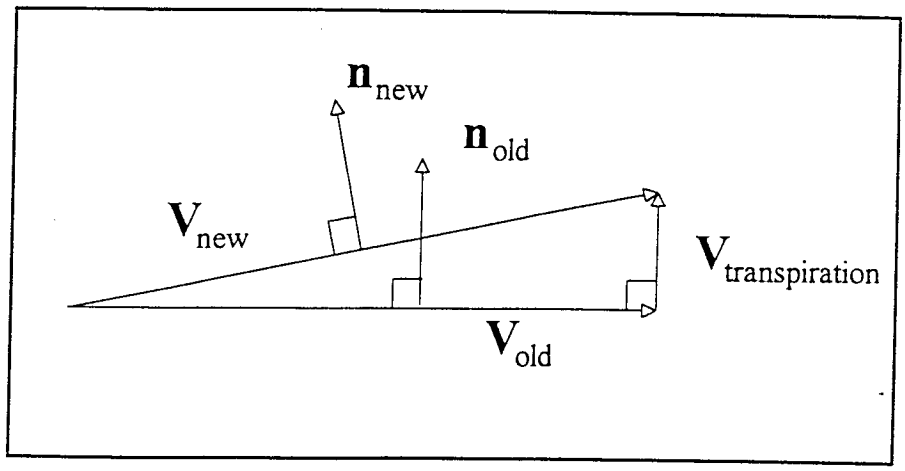

Figure 2.1. Transpiration Implementation

This velocity is then taken as the new tangential velocity. Thus the solution is performed on a seemingly different surface.

2.2. Steady Panel Methods

In general, panel methods use a distribution of singularity elements (e.g. sources and vortices) over a solution boundary to satisfy the solution boundary conditions. This is accomplished by using discrete singularity "panels" over the body surface (and possibly other areas, such as the wake). Combining the velocity potential of each singularity element with that of the freestream, the continuity equation is solved with the proper boundary conditions to give a unique solution for the velocity potential.

One of the conditions that is imposed in a panel method (as in other methods) is flow tangency; that is, there can be no flow through the body surface. Thus, in the solution of a steady panel problem, the boundary condition is

$$\mathbf{V}\cdot\mathbf{n} = 0$$

must be satisfied on each panel, where **n** is the panel normal. To apply transpiration to a panel method, essentially all that needs to be done is to rotate either the panel angle or the panel normal.

The first investigation that was performed used transpiration with a 2D, steady panel code. This code, written by Arena [1993], employs the Smith-Hess panel method. Results were computed for an NACA 0012 airfoil with an actual and a simulated trailing edge flap deflection. In the actual solution, the coordinates of the original airfoil were changed at the flap location to create a 10 degree flap deflection. For the transpiration solution, the angle of each panel in the region of the flap is modified with respect to the free stream in the calculation of the influence coefficients. Thus, a transpiration velocity is not explicitly added, but rather implicitly added by an increase or decrease in panel normal.

2.3. STARS Code

The computer code system used to generate the majority of the comparison data for this study was an extension of the original STARS (STructural Analysis RoutineS) computer program. STARS is an integrated Euler based FORTRAN code for the multidisciplinary analysis of flight vehicles (STARS users manual, 1995). Features of the system include structural analysis, computational fluid dynamics, heat transfer, and aeroservoelastic modules. The most recent version was written under the direction of K. K. Gupta (1995) at the NASA Dryden Flight Research Center primarily to support NASA flight operation, and research and development projects. Until recently, STARS used linearized aerodynamic theory for the prediction of the unsteady flowfields interacting with the elastic motion of an aircraft. This technique produces adequate results for a wide range of problems but has some significant limitations, such as only producing valid results for small perturbation flows. The technique also assumes simple harmonic motion which hinders studies of arbitrary or transient motions.

Due to these limitations, an unsteady Euler CFD module was added which uses transpiration to simulate body surface motion. However, this addition was limited to simulations of single-degree-of-freedom, rigid body, simple harmonic motions. Since a primary responsibility of the STARS group was to calculate aeroelastic effects in support of fight test operations, the program was modified by the STARS group (Gupta, 1995) at NASA Dryden to allow calculation of arbitrary motion and aeroelastic effects.

The code uses finite element analysis to derive the frequencies and mode shapes of the structure. The modal superposition method is then used for the dynamic structural response analysis. The recent addition to the code is a module that enables the

computation of unsteady aerodynamic forces employing the finite element-based structural and computational fluid dynamics computations. This code was validated with theoretical and experimental results.

2.3.1. Flow Solver

The flow solver portion of STARS is an Euler based code capable of simulating three dimensional compressible inviscid flows. It uses finite element techniques with unstructured adapted meshes of tetrahedral elements. The mesh is generated using an advancing front technique, which has the advantages of application to arbitrary shapes, varying grid density in the domain, and the ability of adaptive mesh generation in accordance with solution trend.

The flow solver is comprised of different modules that perform mesh generation and flow solution. The five main modules are as follows:

- SURFACE: generates the two dimensional front
- VOLUME: generates the three-dimensional tetrahedral mesh
- SETBND: sets the boundary conditions on the domain
- EULER_STEADY: performs the steady Euler flow solution
- EULER_UNSTEADY: performs the unsteady Euler flow solution

There is also mesh geometry and flow visualization through the XPLOT and ZPLOT modules of the STARS system. Adaptive mesh techniques are also possible through the module REMESH.

To begin a flow solution study, the user must define the curve components, surface components, curve segments, and surface regions that are necessary to describe the geometry of the problem. The user must also define the background mesh and the nodal spacing parameters. Taking these definitions as inputs, the code automatically generates the surface and volume meshes using the advancing front technique.

The user must then define the boundary condition types for the curves and surfaces to be used by the preprocessor. Finally, the user must create a namelist file that assigns flow conditions and coefficients. The code then takes all of the user input files, plus the files it generates in constructing the mesh and preprocessing the flow information, and performs the steady flow solution. The unsteady flow solution is then performed using the steady flow solution as the initial condition.

2.3.2. Aeroelastic and Aeroservoelastic Solver

The structural solver performs nonlinear, CFD-based aeroelastic and aeroservoelastic analysis. The structural modeling uses a finite element method, thus creating a unified approach using finite element analysis for both the flow and the structural solution. The natural frequencies (ω) and modes (ϕ) are computed by solving

$$M\ddot{u} + Ku = 0$$

where M and K are the inertial and stiffness matrices, respectively, and u is the displacement vector. The steady-state Euler solution is then performed using either an explicit or a quasi-implicit, local time stepping solution procedure that employs a residual smoothing strategy. The equation of motion in the frequency domain is

$$\hat{M}\ddot{q} + \hat{C}\dot{q} + \hat{K}q + \hat{f}_a(t) + \hat{f}_I(t) = 0$$

where

$\hat{M}$ = inertial matrix ($=\Phi^T M \Phi$), and similarly

$\hat{K}, \hat{C}$ = stiffness and damping matrices

q = displacement vector ($=\Phi^T u$)

$\hat{f}_a(t)$ = aerodynamic (CFD) load vector ($=\Phi_a^T pA$), where p is the Euler pressure, A the appropriate surface area, and Φ_a the modal vector pertaining to aerodynamic grid points interpolated from relevant structural nodes

and

$\hat{f}_I(t)$ = impulse force vector ($=\Phi^T f_I$)

where f_I is a number of modes input by the user. The state-space form of the equation is

$$\dot{X} = AX + b_a(t) + b_I(t)$$

where

$$X = \begin{bmatrix} q \\ \dot{q} \end{bmatrix}$$

$$A = \begin{bmatrix} 0 & I \\ -\hat{M}^{-1}\hat{K} & -\hat{M}^{-1}\hat{C} \end{bmatrix}$$

$$b_a(t) = \begin{bmatrix} 0 \\ -\hat{M}^{-1}\hat{f}_a(t) \end{bmatrix}$$

$$b_I(t) = \begin{bmatrix} 0 \\ -\hat{M}^{-1}\hat{f}_I(t) \end{bmatrix}$$

and a time response solution of the state-space equation in an interval Δt ($= t_{n+1} - t_n$) is obtained as

$$X_{n+1} = e^{A\Delta t}X_n + A^{-1}\left[e^{A\Delta t} - I\right]\left[b_a(t_n) + b_I(t_n)\right]$$

The structural deformations u and velocities $\dot{u}$ are then computed and used by the CFD code to change the velocity boundary conditions at the solid boundary. Then a one-step Euler solution using a global time-stepping scheme is performed and the process is repeated for the required number of steps.

2.3.3. Code Modifications

The original unsteady Euler code that was used in this investigation performs surface deflections using transpiration only. If comparisons of these transpiration results

were to be made against actual deflection results, it would be necessary to produce a method of generating a deformed surface mesh. Essentially, the problem reduces to assembling a code that modifies a given surface as desired and a code for calculating the correct normals. Once the deflected surface is obtained with the proper normals, the steady Euler code can be used to perform the flow solution.

The two codes generated to complete the process for obtaining the actual solution were FROMOD and SOLMOD. A flow chart depicting the process is presented in Figure 2.3.

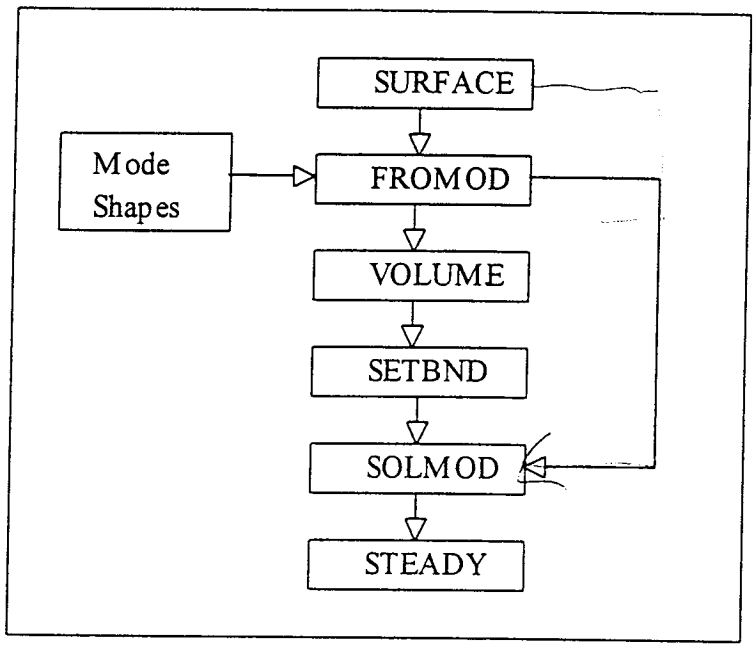

Figure 2.2. Method of Surface Deflection Flowchart

The flow chart shows that the original surface mesh does not need to be modified to deform the surface. A discussion of each code is presented in the follow sections.

2.3.3.1. FROMOD

The three basic components required for performing surface deflection are the original, unmodified mesh, the mode shapes of the different modes, and scaling factors specifying the generalized displacements. The unmodified mesh can be obtained by generating the mesh on the original surface. The mode shapes are obtained from the finite element structural solver. The final requirement is a set generalized displacements, which is provided by the user.

The original surface is altered by displacing each node point in each coordinate direction, x, y, and z, on the surface by an amount that is determined from the mode shapes and their generalized displacements. For example,

$$x_{new}(i) = x_{old}(i) + \Delta x(i)$$

where $\Delta x(i)$ is determined by

$$\Delta x(i) = \sum_{j=1}^{n} \Phi_a(i,j) * f_I(j)$$

where $\Phi_a(i,j)$ is an array of mode shapes

$f_I(j)$ is an array of generalized displacements, input by the user

and n is the number of modes

Essentially, FROMOD is used to generate a deformed surface mesh. It reads in the surface definition and the generalized forces and prompts the user for the modal scaling factors. Using this data, the code generates an array of nodal displacements and adds these displacements to the original nodes, as previously described. Then the code writes the new surface file. One advantage of this procedure is that the connectivity of the surface is unchanged, so it can simply be transferred from the old surface file to the new one. The final requirement is a code to calculate the normals for the deflected surface. This code is discussed in the following section.

2.3.3.2. SOLMOD

A second modification code was required to complete the process for determining actual deflection solutions. This code, called SOLMOD, was needed to calculate the surface normals for the new mesh. SOLMOD reads in the file containing the normals, corrects the normals, and then overwrites the old normals file with the new one.

The computational process for modifying the normals already existed in the Euler code because it is used in the transpiration solution. In this process, the normals at each node in the mesh are calculated using an area weighted average of surface triangulations that contain that node. Since this coding was already present, it was simply combined with the proper read and write statements to create SOLMOD.

CHAPTER 3

RESULTS

The main objective of this study was to determine the effectiveness of the transpiration boundary condition in unsteady aeroelastic applications. This was to be done by performing investigations of various geometries over a wide range of Mach numbers. By doing so, this boundary condition could be employed in the prediction of flutter boundaries. The rationale is to discuss the instances in which transpiration will introduce error into the solution, and to generate comparison data to show the effectiveness of transpiration in various applications. The following section contains a discussion of the limitations. Subsequent sections present results demonstrating the capability of transpiration.

The first set of results that is presented is for a steady, trailing edge flap deflection, as a preliminary investigation. The next two sets of results comprise the core of the research, the first being a 2 by 1 flat plate and the second being the AGARD 445.6 wing. In these cases, solutions were performed for actual deflections and compared to simulated deflections using transpiration. The final cases of the study address the issue of mesh sensitivity in computational fluid dynamic solutions.

3.1. Transpiration Limitations

The idea of transpiration is essentially to alter the boundary condition when performing a flow solution. In using transpiration, if the surface under investigation deflects, the surface normals are modified to account for the deflection. Therefore, if the deflection is small, transpiration can very accurately predict the solution. This is because the relative position of one part of the surface to another will have little effect. However, as the deflection increases, the accuracy of the transpiration solution will decrease. Since transpiration only accounts for the orientation of the normals, the effect of translation between two points on the surface will not be accounted for in the solution.

As an example of this translation problem, consider a wing that has first mode bending such that the free end is no longer in the same plane as the fixed end. When transpiration is used to simulate the bend, the normals along the wing will be altered in the wing's original position. Thus the effect that a point on the displaced end has on points elsewhere will not be completely accurate, and increasing the displacement will add to the inaccuracy.

One consequence of the translation effect is error introduced by intersecting shocks and surfaces. Consider a shock wave originating at the nose of an aircraft whose wing is oscillating in first mode bending. In the transpiration solution, the shock will

intersect the wing in its original position. However, in the actual solution the wing is displaced, thus the shock intersection will not be in the same location.

Other problems such as this could result when there is internal surface translation of the body under investigation. As mentioned, however, in cases of small deflection, such as in flutter problems, transpiration can produce very accurate results.

3.2. Steady Flap Case

In order to gain a better understanding of the transpiration concept and to perform some preliminary investigations, a panel code was modified to employ transpiration. Actual and simulated surface pressures were computed for a N0012 airfoil at Mach 0.6 and zero degree angle of attack with a steady 10 degree flap deflection. The results were obtained using a FORTRAN code written by Arena that employs the Smith-Hess panel method. Slight modifications to the code were made to obtain the transpiration results. Figure 3.1 shows the deflected flap, located at 80% of the chord.

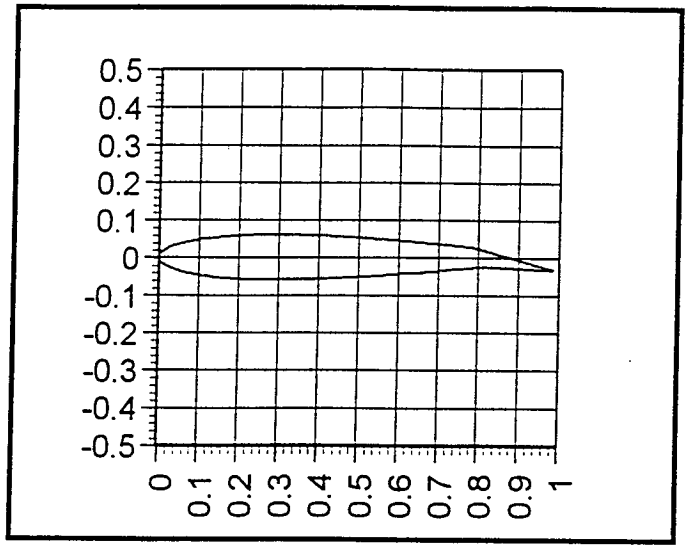

Figure 3.1. NACA 0012 Airfoil with Deflected Flap

Actual and simulated surface pressures were generated using the Smith-Hess code. These pressures were corrected for compressibility effects using Prandtl-Glauert correction. The corrected results are presented in Figure 3.2.

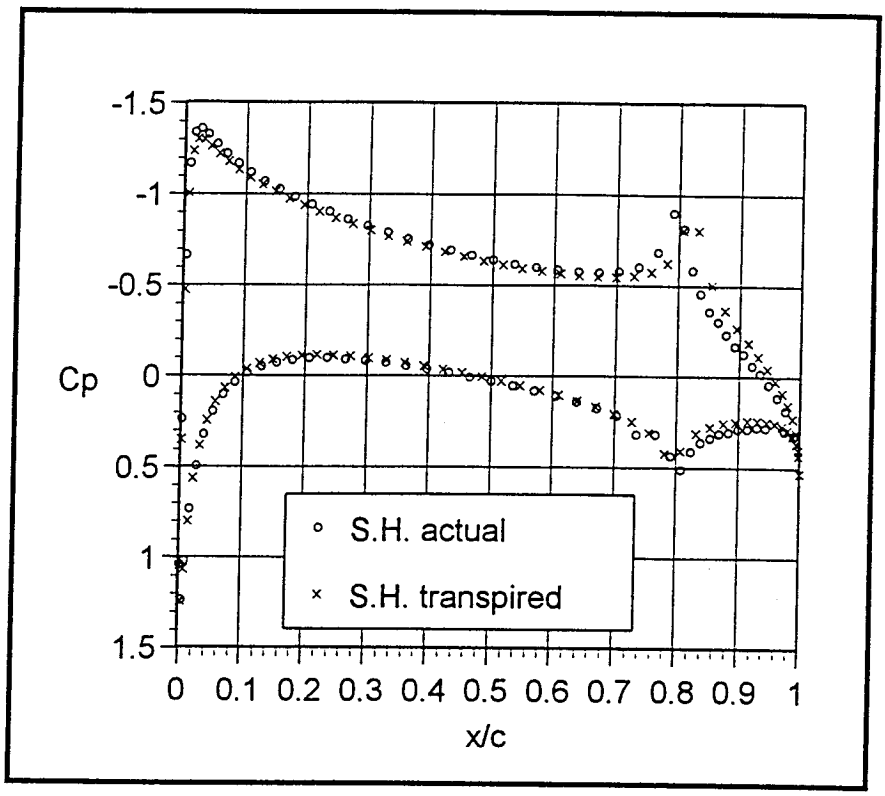

Figure 3.2. NACA 0012 Surface Pressure Results from Panel Code

It can be seen from Figure 3.2 that transpiration is very effective in simulating the flap deflection with only slight differences occurring near the flap-airfoil intersection.

This study was also performed by Raj using a steady Euler method that also employs transpiration. In that study, transpiration results were also compared against actual flap deflection results. Figure 3.3 shows the actual and transpiration simulated results obtained by both the Smith-Hess code and by Raj.

One of the primary cases in this investigation involved a flat plate 2 units long and 1 unit wide. This type of plate is representative of configurations that have been used in well documented studies on panel flutter. As defined by Dixon , panel flutter is a self-excited oscillation of the external surface skin of a flight vehicle which results from the dynamic instability of the aerodynamic, inertia, and elastic forces of the system. Information gained from studies involving panel flutter has assisted in the pursuit for flight vehicles with increasing speeds. This investigation of panel flutter is gives a new approach to this well known problem, as it allows for flutter investigations in which the surface under consideration is never required to actually deform.

The plate used in this study was centered on a surface 4 units long by 3 units wide. This plate and the surface mesh are shown in Figure 3.4.

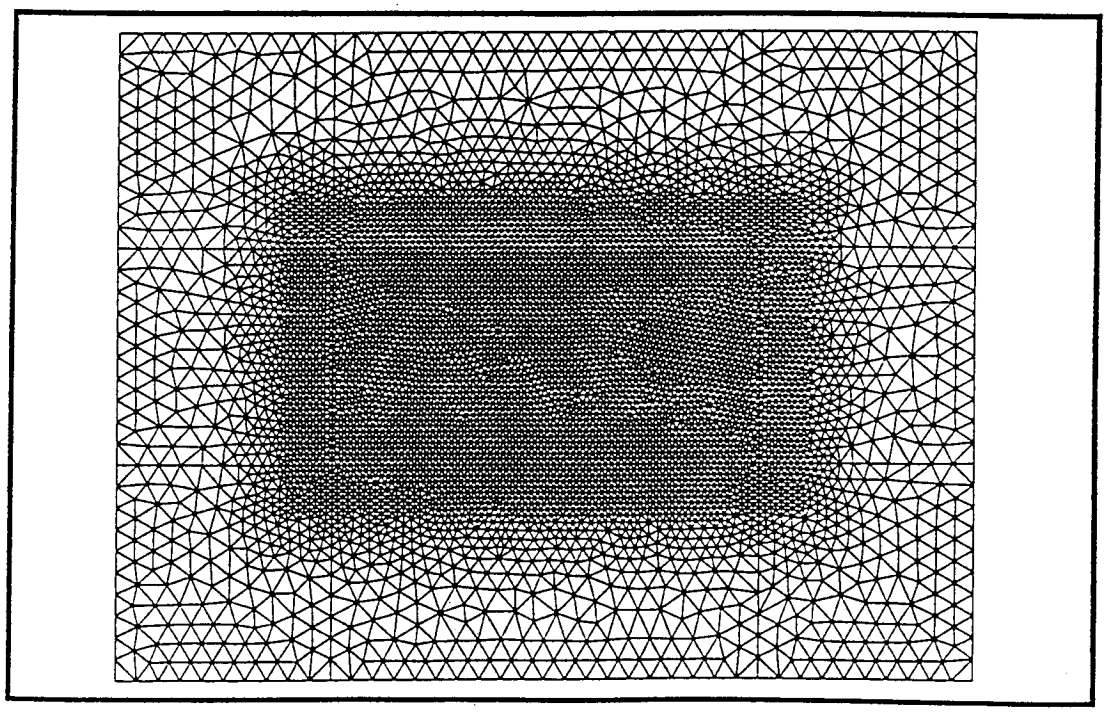

Figure 3.4. Surface Mesh for Plate Case

This figure shows that the grid resolution on and immediately around the plate is very high. This was necessary to generate a smooth flow solution over the plate. The freestream flows over the top of the plate, with both sides of the plate being at atmospheric pressure. The plate edges are pinned to the bottom surface. All surfaces are defined as walls and all edge boundaries are defined as far field. The plate is flat, but can be made to deform, as described by Section 2.3.3, or deformation can be simulated using transpiration. The deflection can be any combination of six bending modes of the plate. In plate flutter, the magnitude of deflection in each mode would not necessarily be the same. However in this study, all modal deflections were of equal magnitude for an arbitrary deflection.

The first case compares actual and transpiration results for a generalized displacement of 0.1 in all modes. As an illustration, each mode shape is shown separately in Figure 3.5.

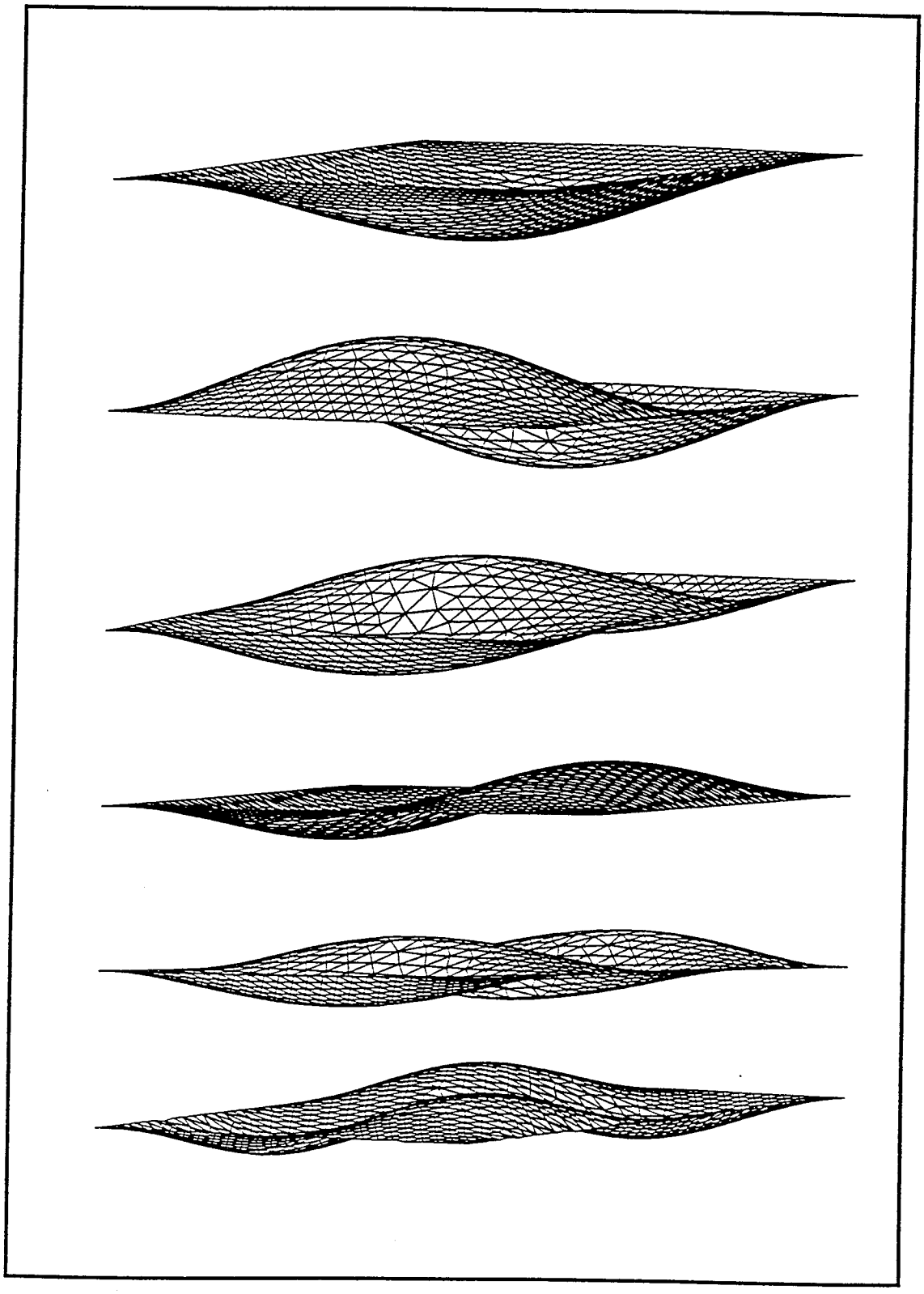

Figure 3.5. Six Vibrational Modes for Plate Case

The superposition of modes that produced the surface used in this case is presented in Figure 3.6.

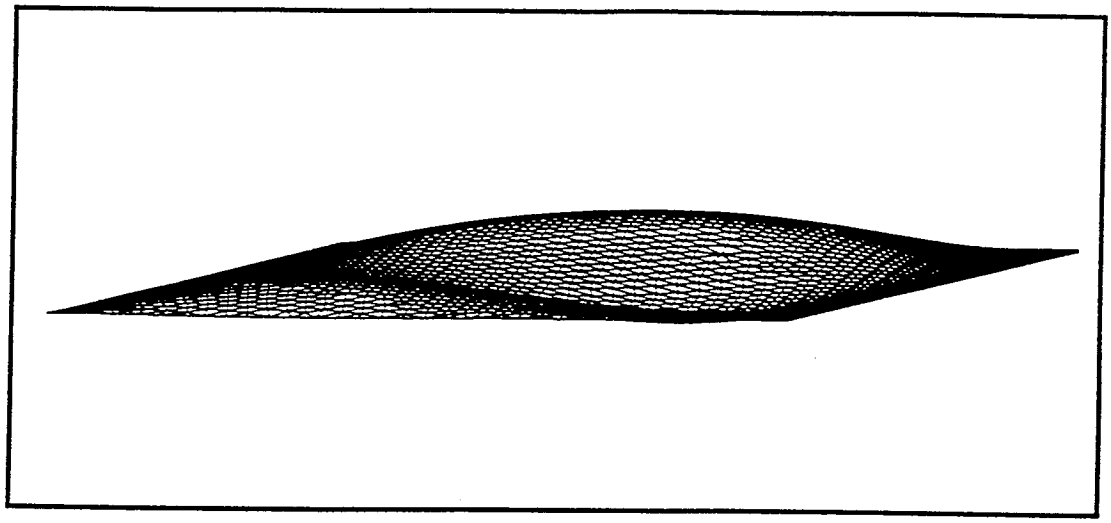

Figure 3.6. Deflected Plate Surface

The resulting deflection produces a maximum deflection that is over 7% of the width of the plate. This case was selected as an initial attempt to determine limitations of transpiration. Arbitrary deflection was used to maintain generality; 0.1 amplitudes were used to give a significant deflection. Surface pressures and generalized forces were compared for freestream Mach numbers 0.3, 0.95, and 3. In all cases, the actual and simulated surface pressures were very similar. The generalized forces were comparable, but did show some appreciable differences.

Figures 3.7 and 3.8 show actual and transpiration surface pressure contours, respectively, for the Mach 0.3 case.

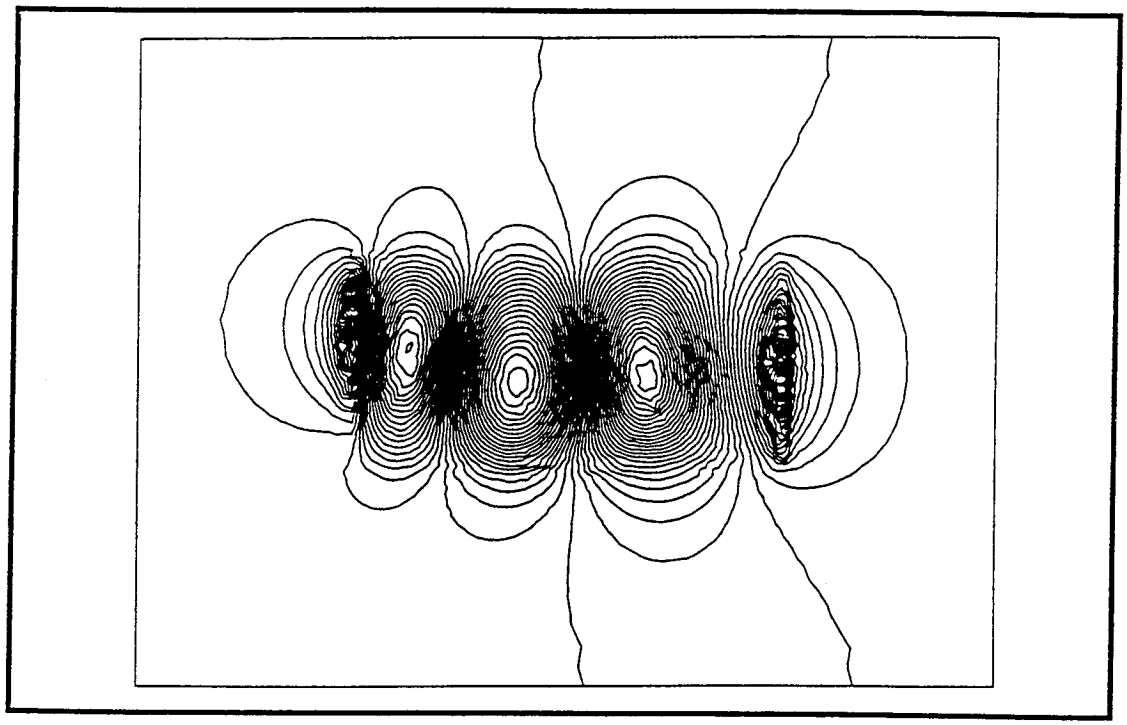

Figure 3.7. Actual Pressure Contours, Mach 0.3

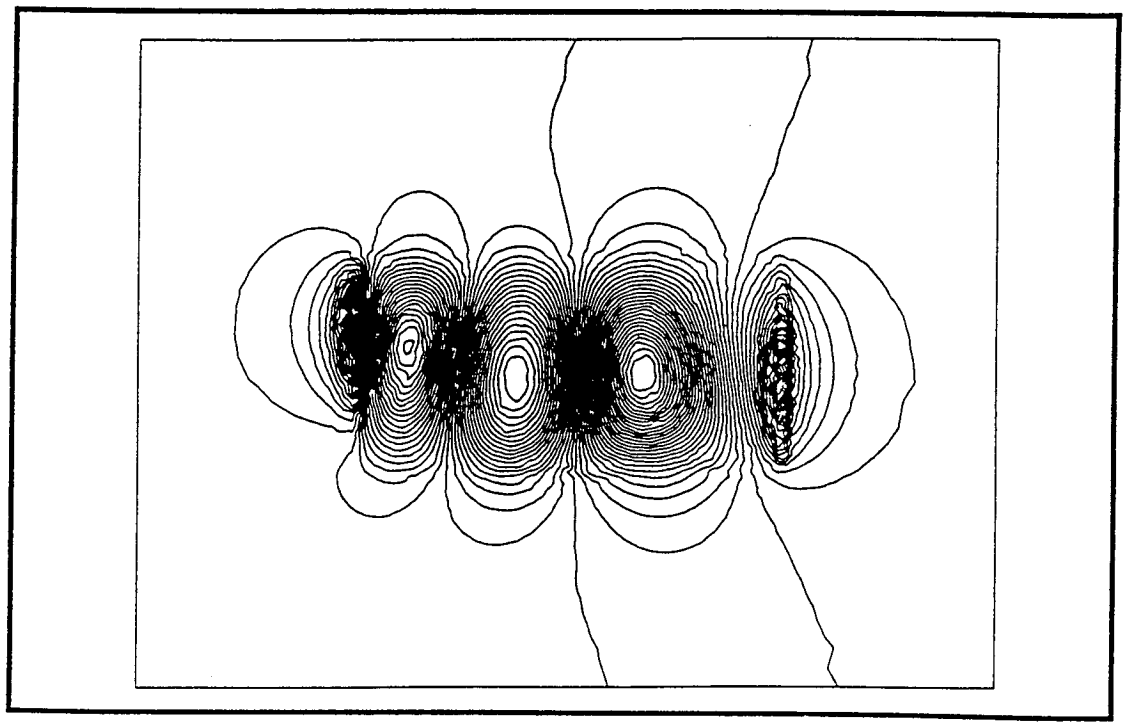

Figure 3.8. Pressure Contours Using Transpiration, Mach 0.3

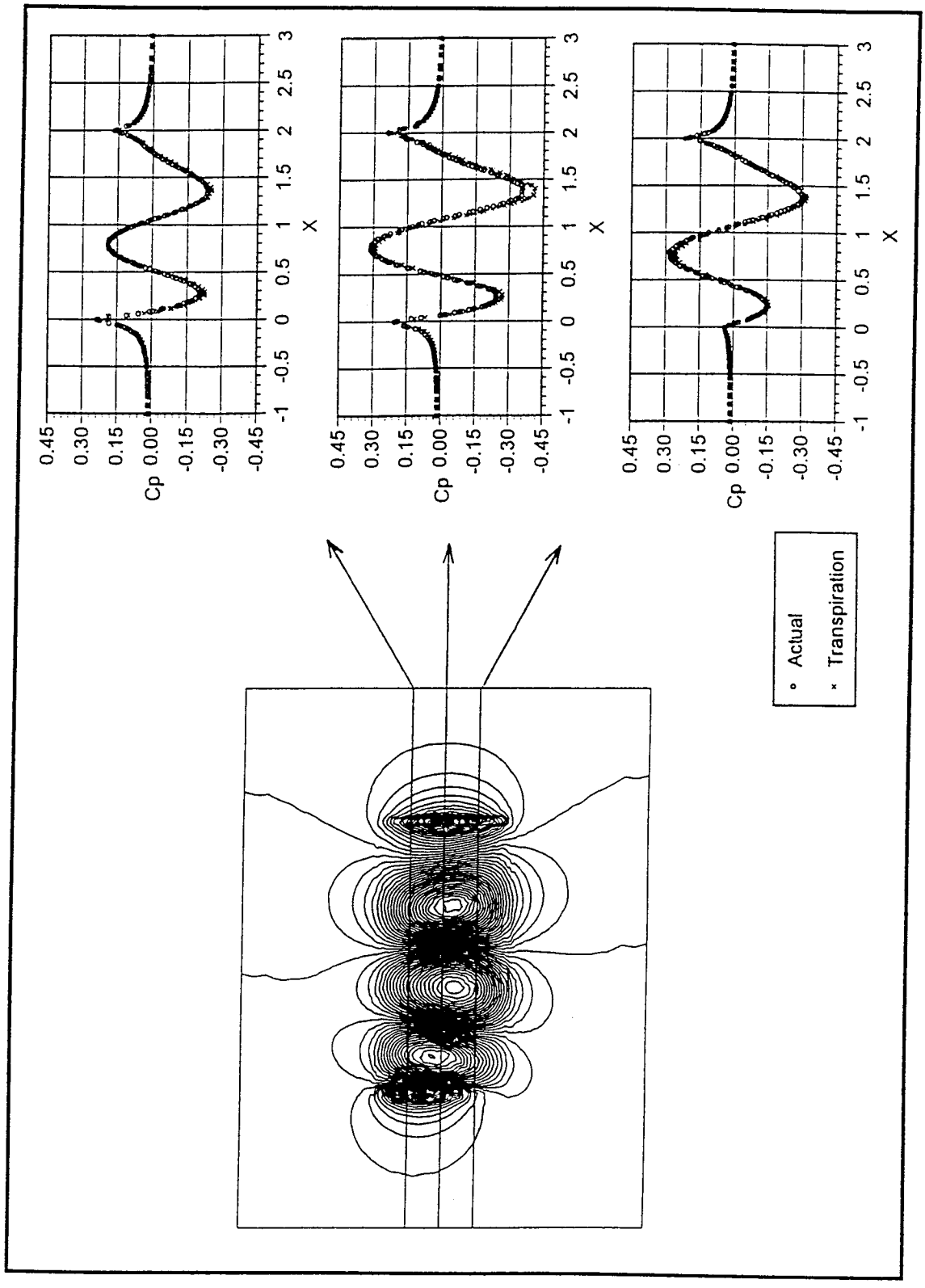

Figure 3.10. Pressure Profiles, Mach 0.3

These pressure profiles show that there is very good agreement between the two results. The largest differences appear to be in regions where the plate is furthest displaced from its original position, which would be expected. Table 3.1 shows the generalized forces for the six modes of each case.

Table 3.1. Generalized Forces for Mach 0.3

Mode	Actual	Transpiration
1	-22.14	-41.66
2	-87.48	-91.38
3	-54.55	-57.12
4	-4.649	-2.229
5	17.65	18.56
6	-57.16	-58.33

The generalized forces are very comparable except in modes 1 and 4. Large differences in generalized forces will be discussed at the end of this section.

The surface pressure contours for the Mach 0.95 case are shown in Figures 3.11 and 3.12.

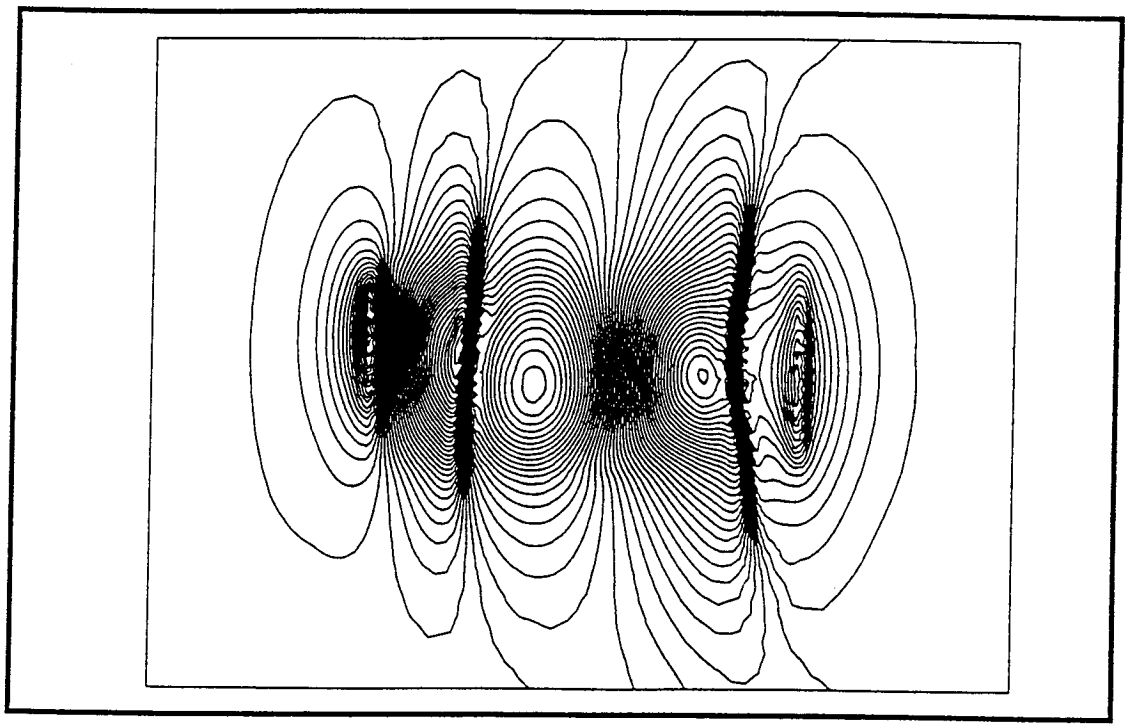

Figure 3.11. Actual Pressure Contours, Mach 0.95

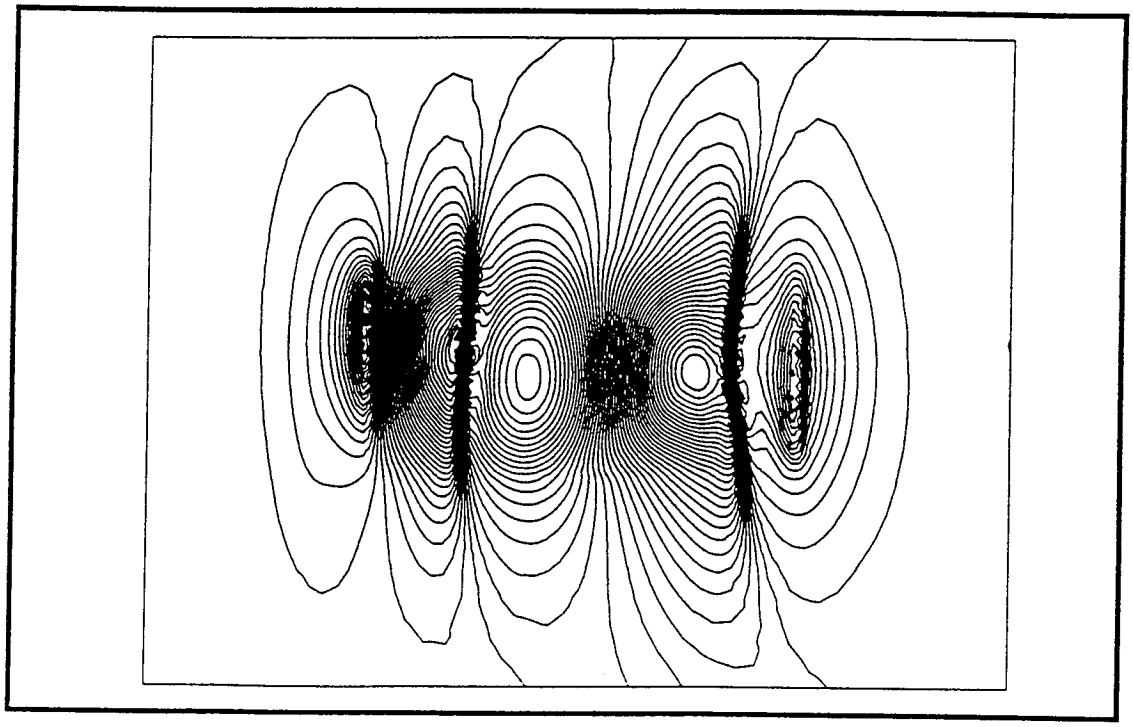

Figure 3.12. Pressure Contours Using Transpiration, Mach 0.95

Again, the pressure contours in each case are very similar. The pressure profiles for this Mach number are presented in Figure 3.13.

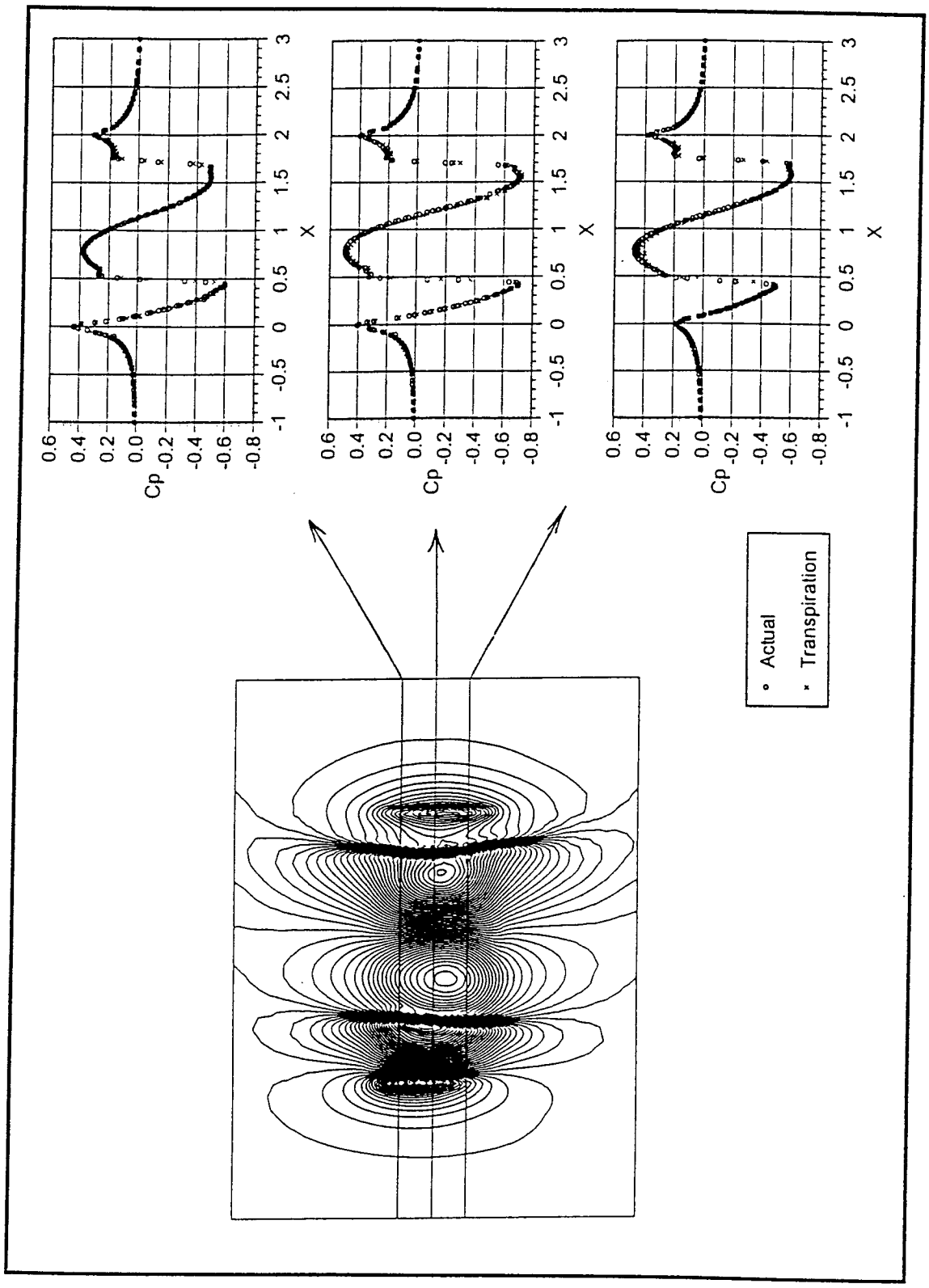

Figure 3.13. Pressure Profiles, Mach 0.95

These pressure profiles show excellent agreement between the two data sets with only slight differences being seen near some pressure peaks and in some regions of sharp pressure changes. The transpiration solution also seems quite capable of handling the formation of the two shocks. This can be seen again in the Mach profiles at the same locations in Figure 3.14.

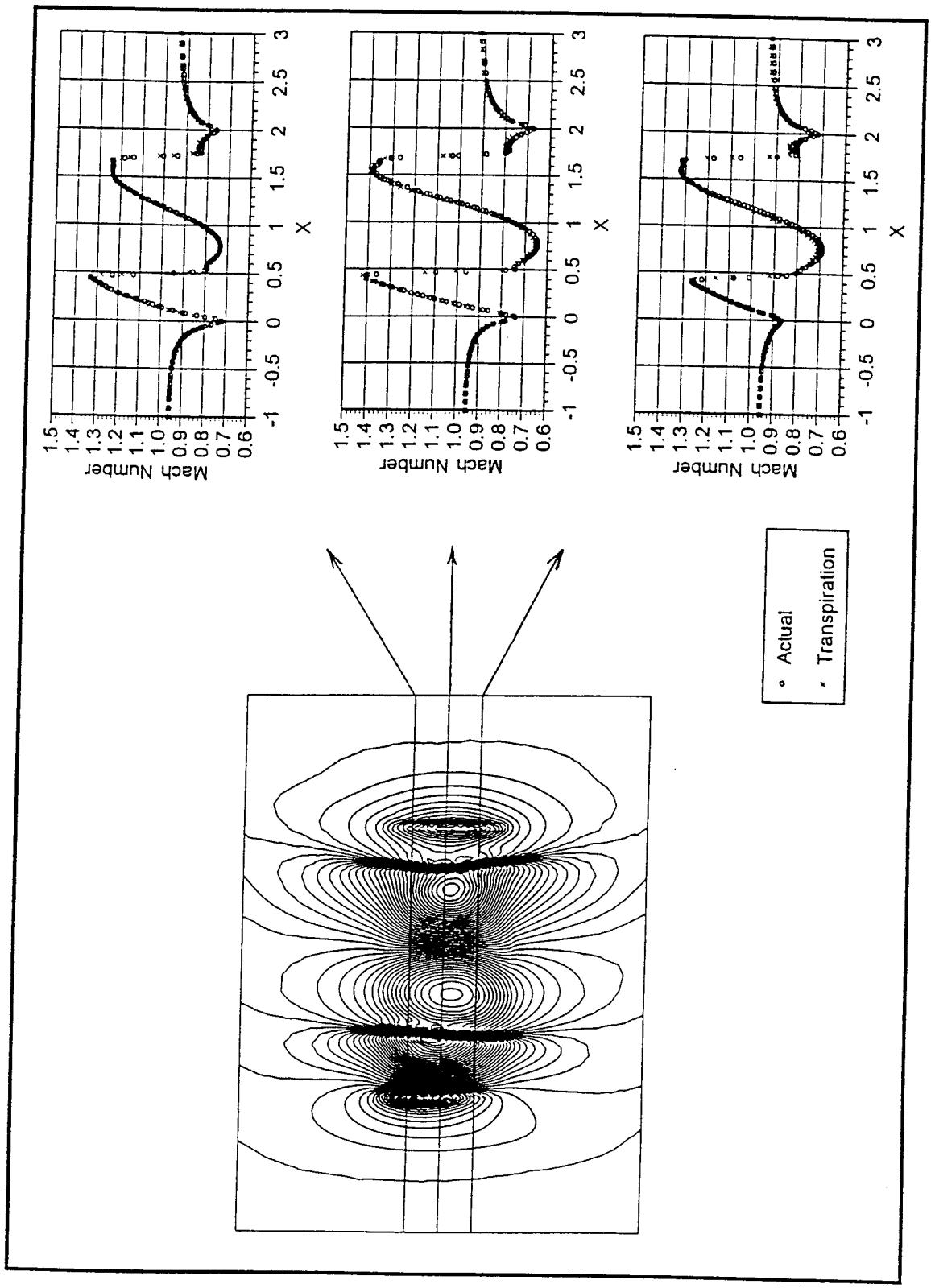

Figure 3.14. Mach Profiles, Mach 0.95

Notice how there are only minor difference near the shocks, and seemingly no differences at the shocks. The generalized forces for this case are presented in Table 3.2.

Table 3.2. Generalized Forces for Mach 0.95

Mode	Actual	Transpiration
1	-283.2	-475.1
2	-1457	-1483
3	-1500	-1495
4	-61.35	-34.72
5	233.5	236.3
6	-869.1	-886.9

These forces are also comparable, with some noticeable differences again being seen in modes 1 and 4.

Figures 3.15 and 3.16 show the surface pressure contours for the Mach 3.0 case.

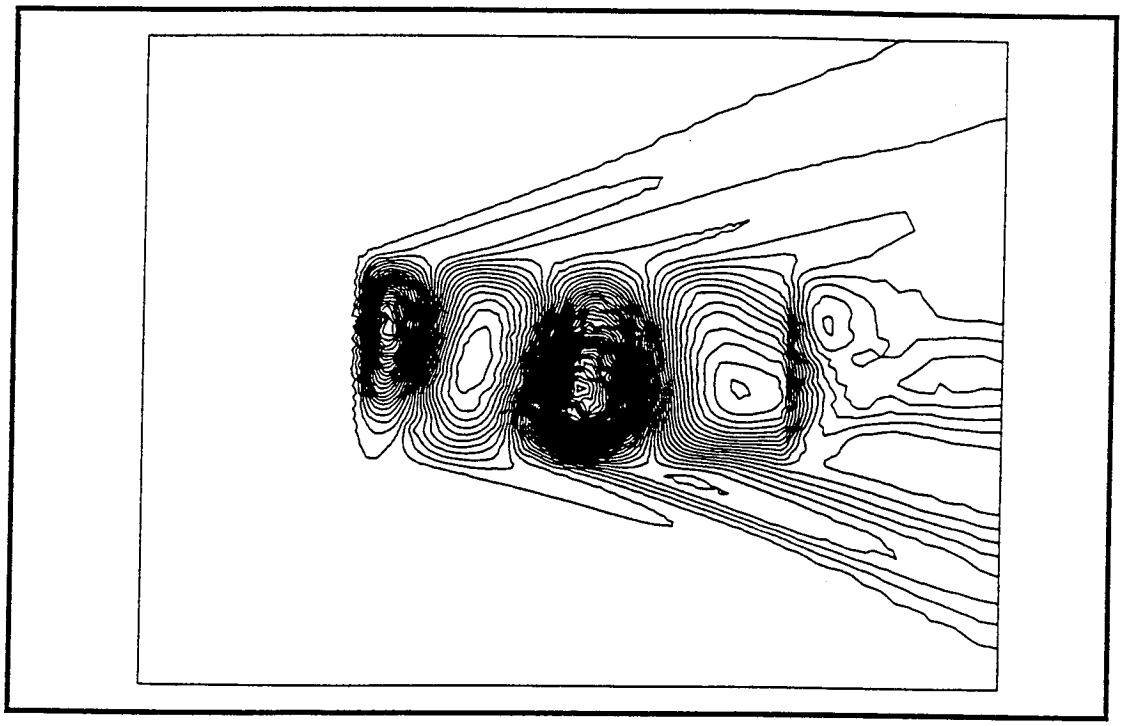

Figure 3.15. Actual Pressure Contours, Mach 3.0

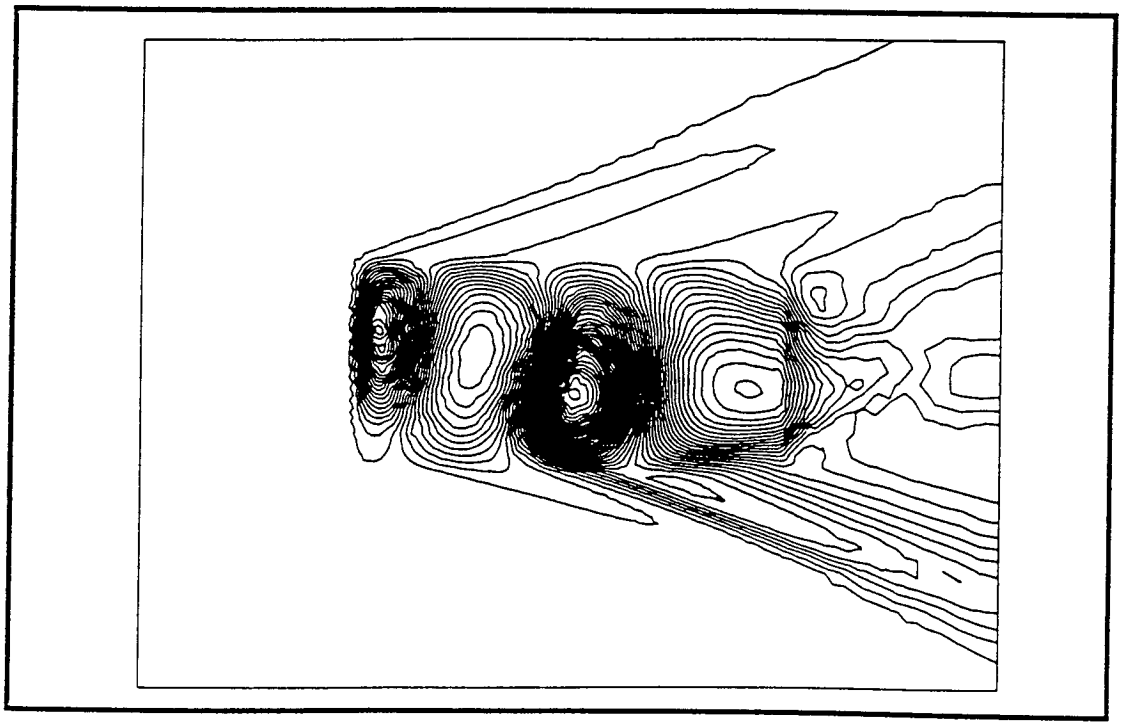

Figure 3.16. Pressure Contours Using Transpiration, Mach 3.0

As in the two previous cases, the pressures appear to be very much alike. Figure 3.17 shows the pressure profiles.

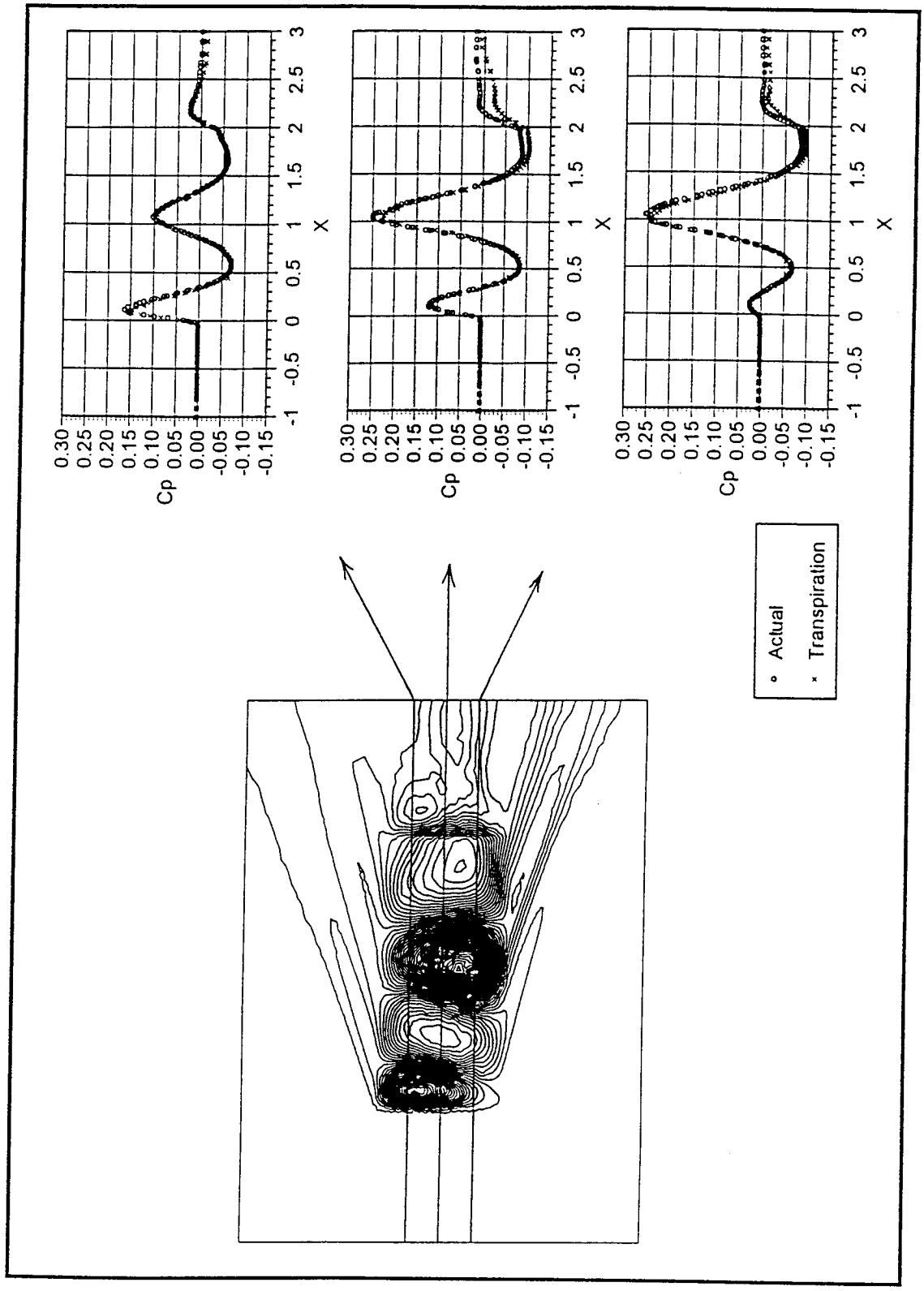

Figure 3.17. Pressure Profiles, Mach 3.0

Most regions show good results, however, some interesting differences can be seen in the region near the end of the plate. These differences could be due to the abrupt change in slope where the plate ends, since the edges of the plate are pinned and not clamped. Table 3.3 gives the generalized forces for this case.

Table 3.3. Generalized Forces for Mach 3.0

Mode	Actual	Transpiration
1	2593	2041
2	534.7	253.1
3	-3708	-3826
4	-848.3	-809.4
5	-574.8	-373.4
6	2248	2194

Here, the differences in generalized forces are seen in modes 2 and 5.

As an illustration of one of the criterion for convergence, the residuals for this case are presented in Figure 3.18.

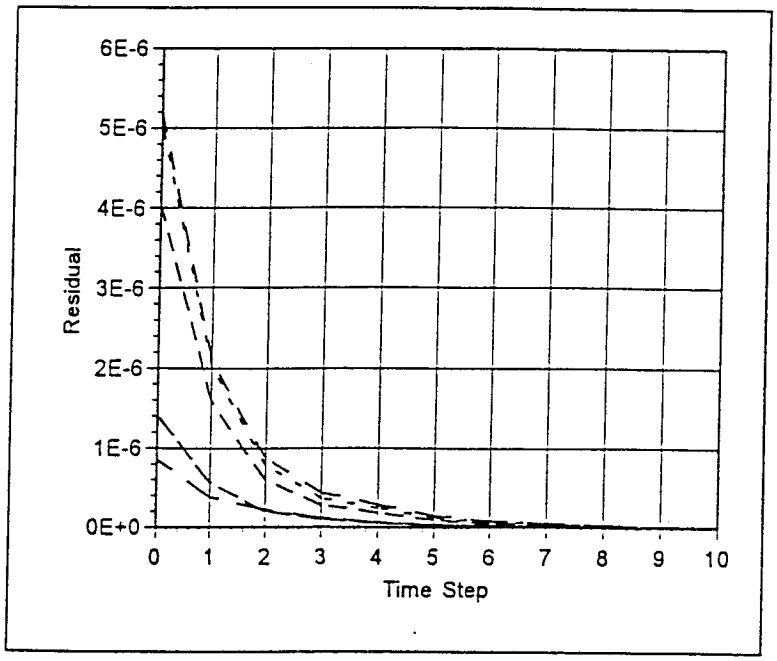

Figure 3.18. Residual Convergence

This shows a well converged solution with final residual values being on the order of 10^{-10}.

It is evident from these plots that transpiration very accurately simulates the deflection. However, this is not readily assumed when studying the generalized forces. Since the surface pressures match so closely, it can be deduced that generalized forces may be very sensitive to small differences in surface pressures. However, differences may be negligible if the structural spring force is large relative to the generalized forces. Also, since in one case there is actual plate deformation while in the other case the deflection is only simulated, the internal mesh of each domain will be different. Subsequently, as will be shown in later sections, the solution can be strongly dependent on the mesh. Therefore,

not all of the differences seen can necessarily be attributed to the transpiration boundary condition.

3.4. AGARD 445.6 Wing

The next case that was investigated was the AGARD 445.6 wing. This wing is a standard aeroelastic test configuration which has been investigated experimentally in the Langley Transonic Dynamics tunnel. Using this wing allows for transpiration comparison in practical application. Also, in this case, the surface is surrounded by the flow unlike the plate case where the flow is only on one side, thus adding to the complexity of the problem. The original, undeflected wing is shown in Figure 3.19.

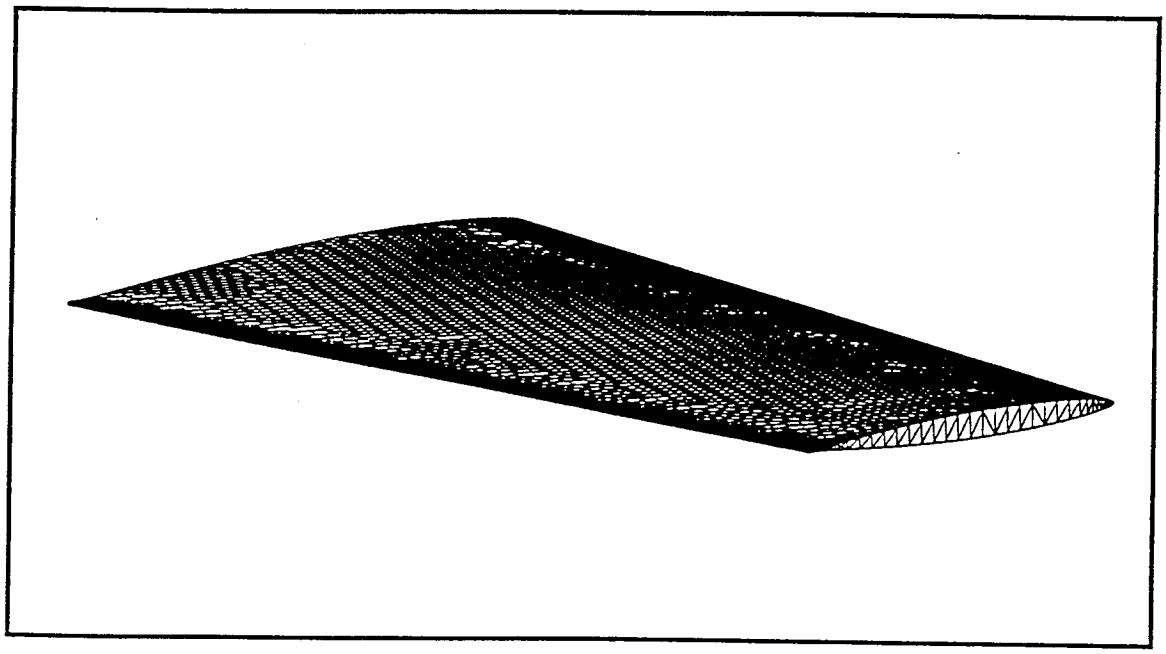

Figure 3.19. AGARD Wing

The wing was given a generalized displacement of 2 units in first mode bending and 2 units in first mode torsion. The deflected wing is shown in Figure 3.20.

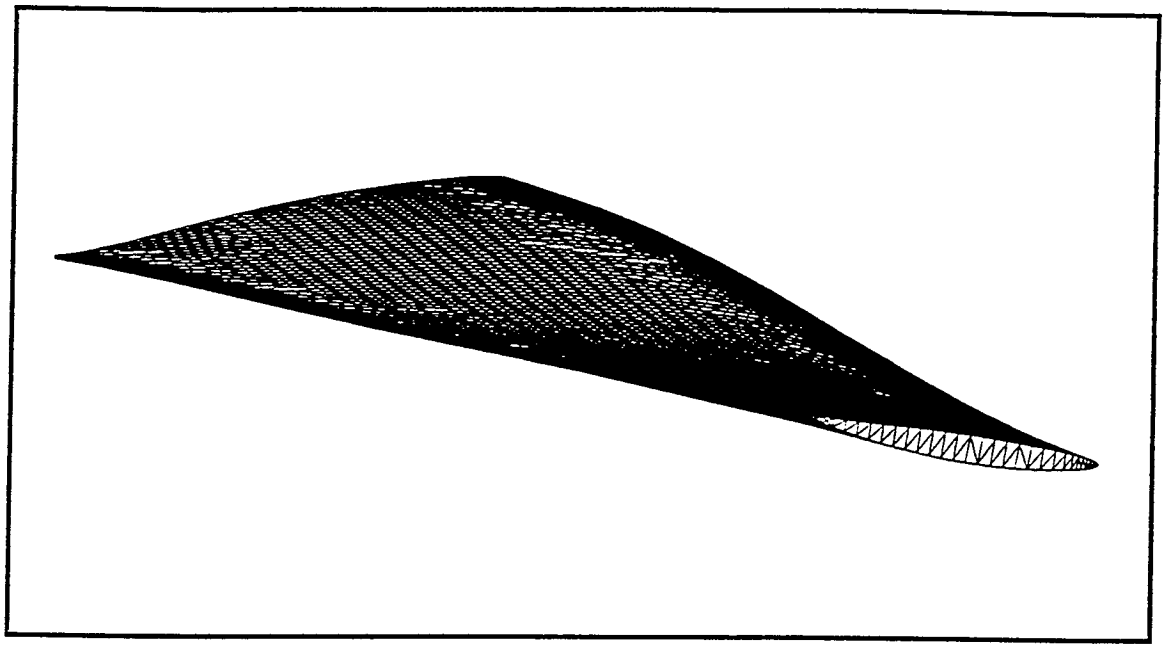

Figure 3.20. Deflected AGARD Wing

The severity of the deflection is apparent from this figure. It is so significant that an approximate -9 degree angle of attack is created at the tip of the wing where there should be none. In addition, the end of the wing has translated below its original position. Results were obtained for Mach numbers of 0.99, 1.141, and 2.0, using this deflection. Even with this unrealistic deformation at these Mach numbers, transpiration produces a very accurate simulation.

The surface pressure contours on the lower surface of the wing for Mach 0.99 are shown in Figures 3.21 and 3.22.

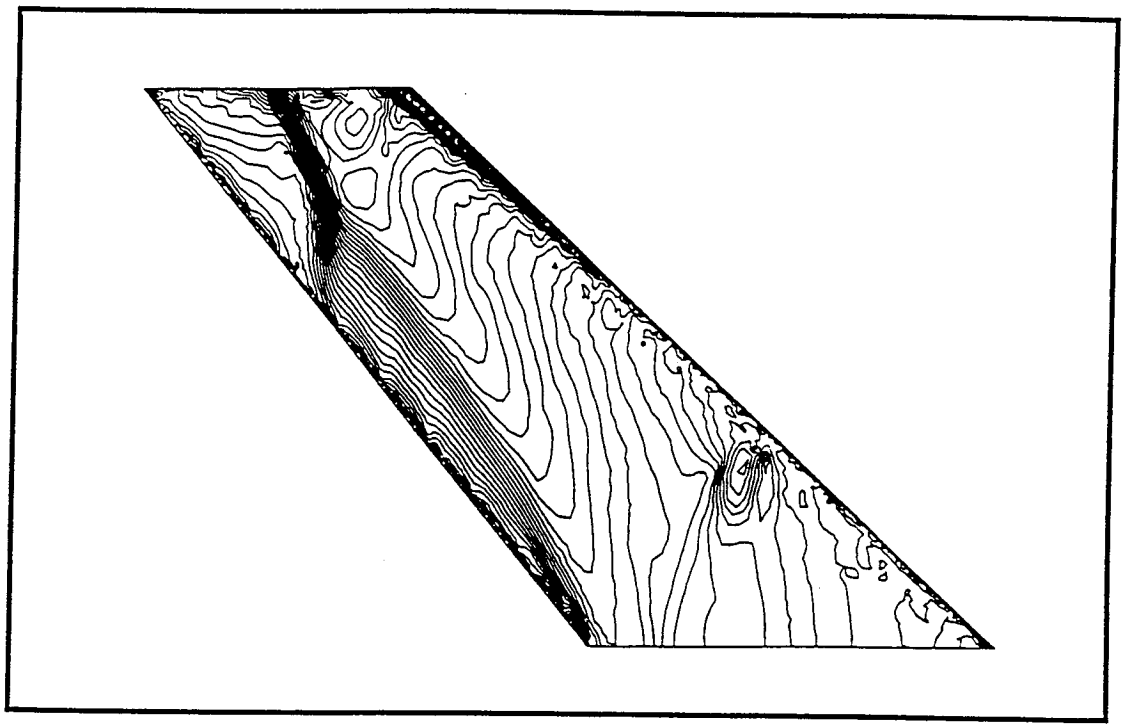

Figure 3.21. Actual Pressure Contours, Mach 0.99

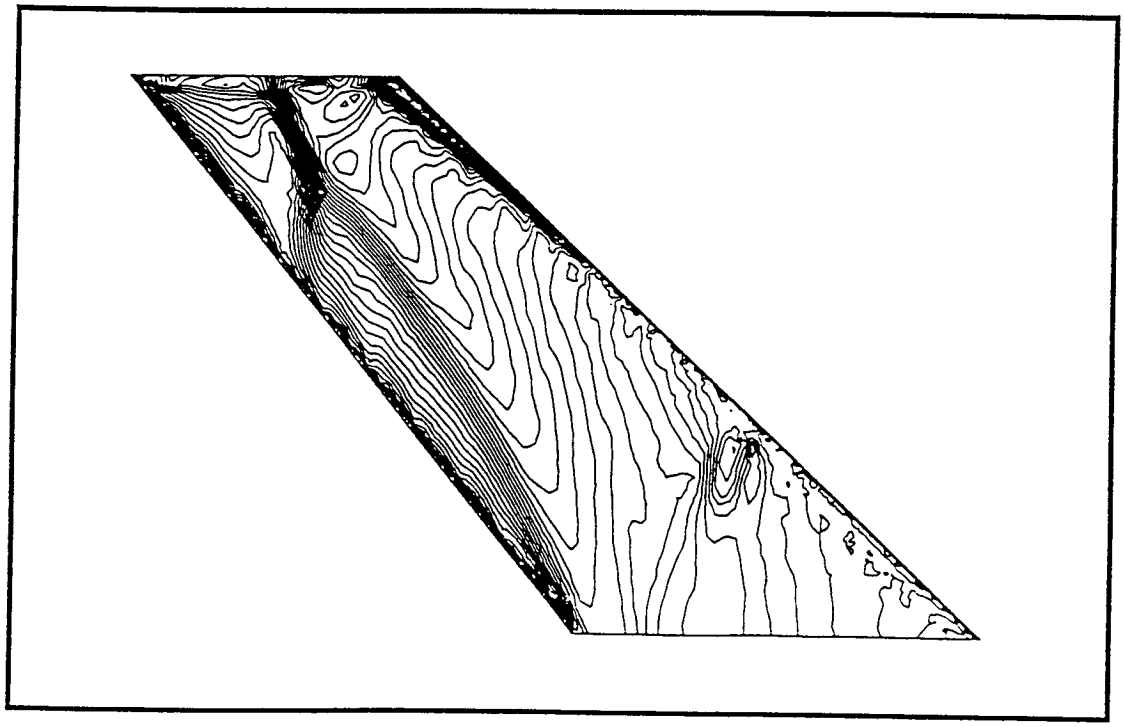

Figure 3.22. Pressure Contours Using Transpiration, Mach 0.99

Both results show the same regions of strong pressure gradients and both predict the formation of a shock near the middle of the tip of the wing.

Actual and simulated surface pressure profiles at three stations for the Mach 0.99 are shown in Figure 3.23.

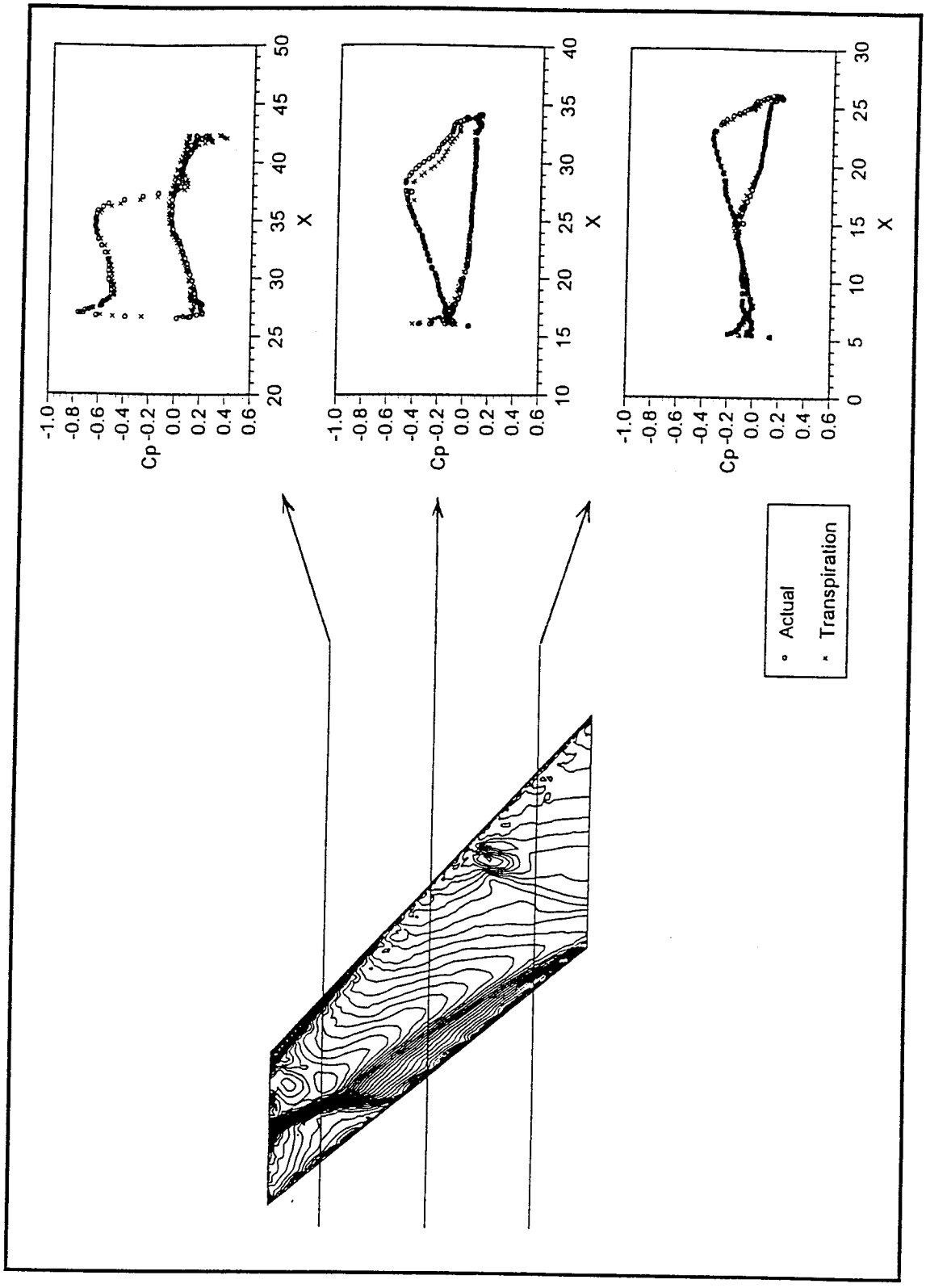

Figure 3.23. Pressure Profiles, Mach 0.99

The two data sets show very good agreement near the root of the wing. There is also good agreement near the tip of the wing except very close to the trailing edge, where the transpiration solution predicts a larger pressure peak. The largest differences are seen at the middle of the wing where the data is somewhat shifted near the trailing edge.

Surface pressure contours are presented for the Mach 1.141 case in Figures 3.24 and 3.25, again for the lower surface.

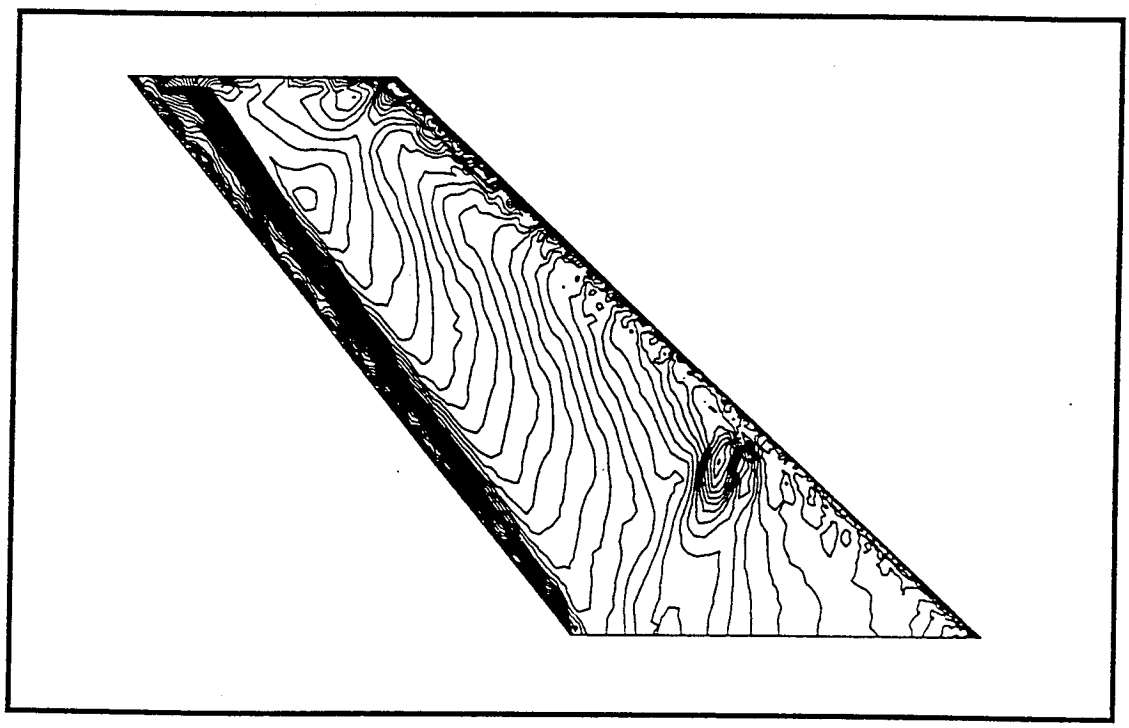

Figure 3.24. Actual Pressure Contours, Mach 1.141

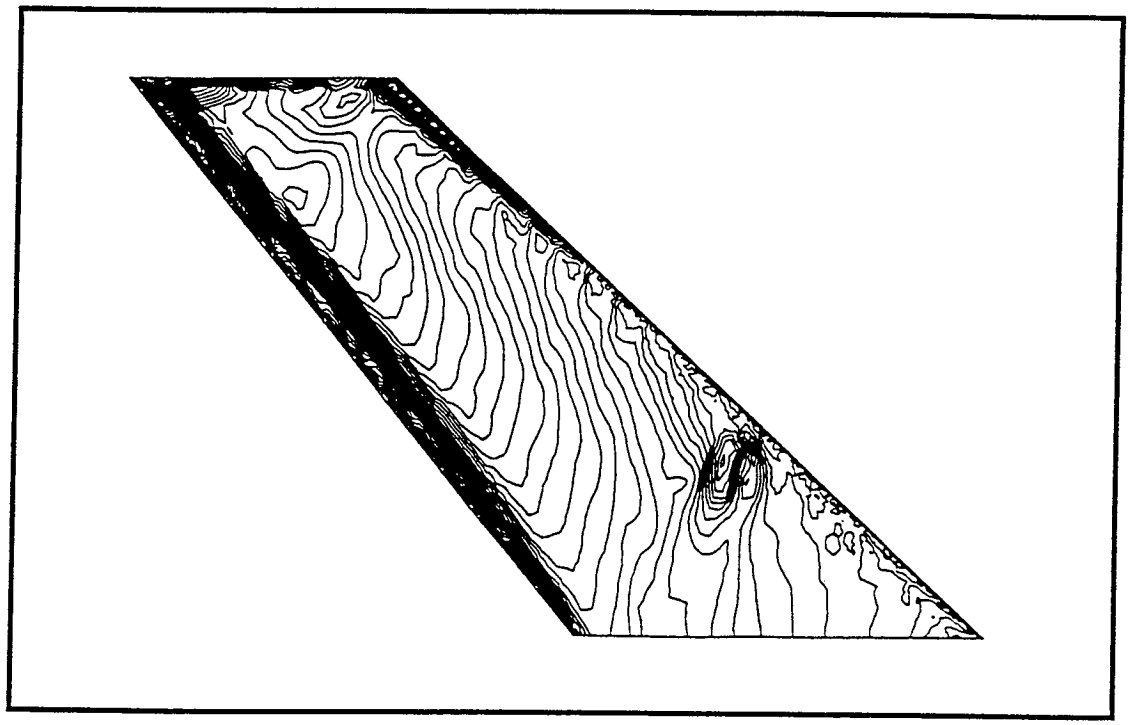

Figure 3.25. Pressure Contours Using Transpiration, Mach 1.141

Overall, the results appear to be very good from studying the pressure contours. The pressure profiles for this case are presented in Figure 3.26.

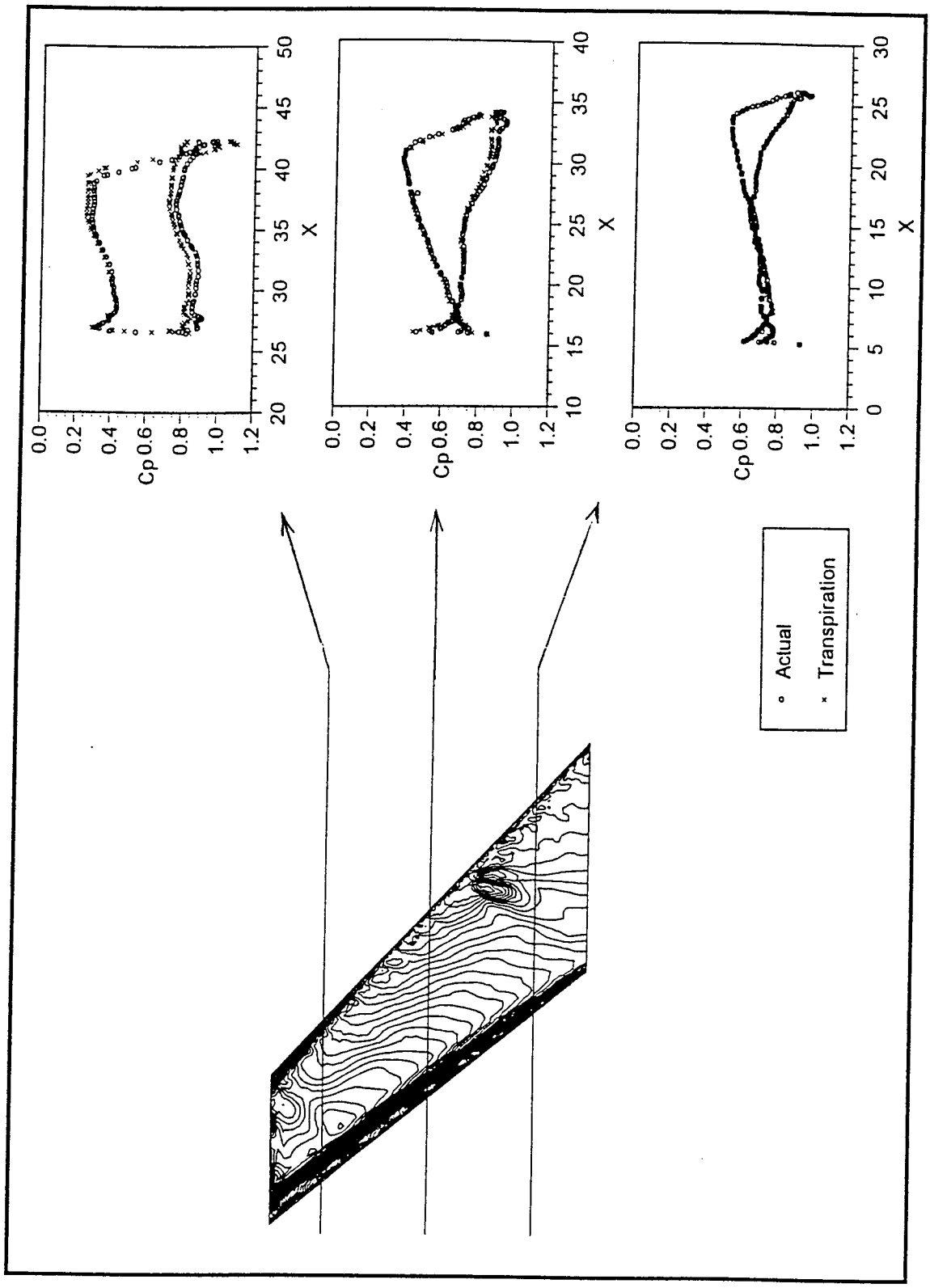

Figure 3.26. Pressure Profiles, Mach 1.141

Results near the root of the wing are extremely good, except for a slight difference in pressure peaks at the trailing edge. The agreement decreases with increasing distance from the root. This demonstrates the limitation described in Section 3.1 of transpiration not accounting for actual surface translation, since the wing is increasingly displaced from its unmodified position moving from wing root to tip. However, despite the very large deflection and rotation at the tip, the results there are quite good, with the largest percent error being less than 15%.

The surface pressure contours on the lower surface for the Mach 2.0 case are shown in Figures 3.27 and 3.28.

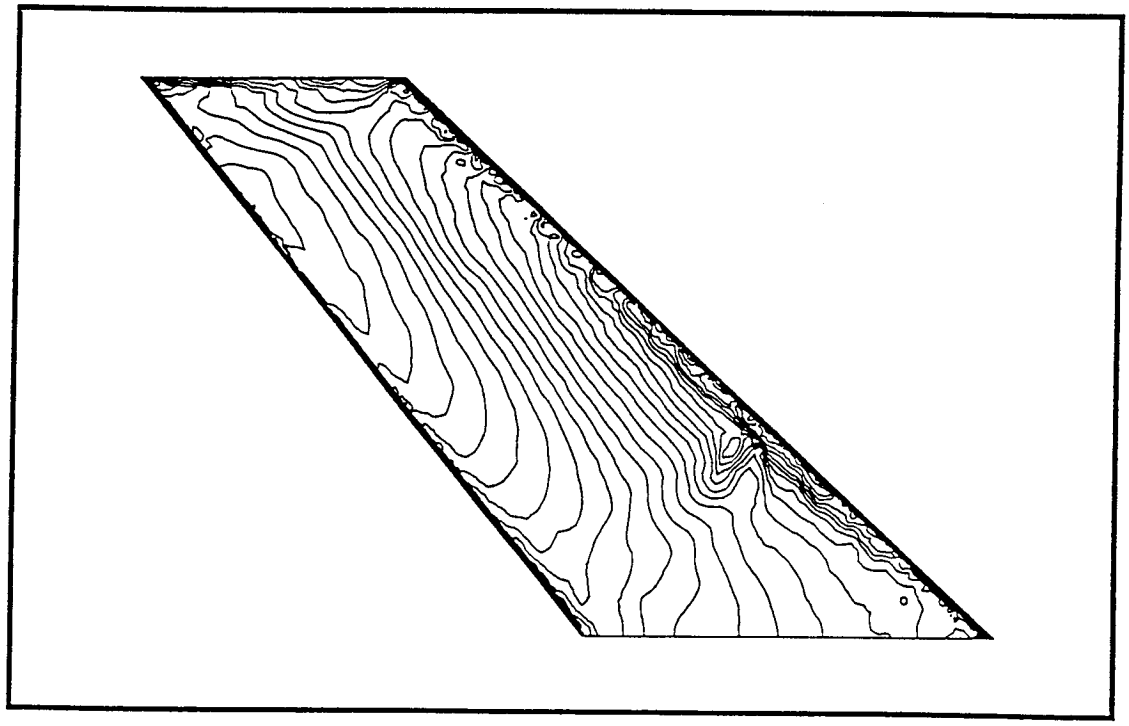

Figure 3.27. Actual Pressure Contours, Mach 2.0

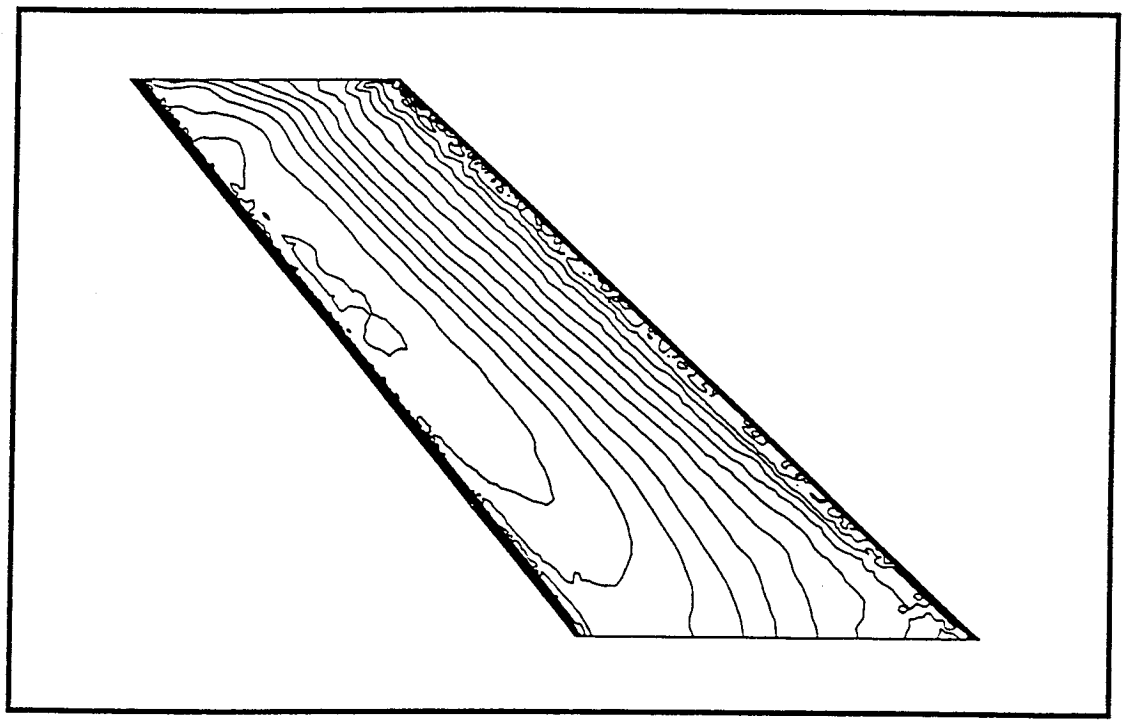

Figure 3.28. Pressure Contours Using Transpiration, Mach 2.0

Strong pressure gradients can be seen near the leading and trailing edges in both cases. The pressure change from leading edge to trailing edge appears to be more uniform in the transpiration case than in the actual deflection. However, in both cases the pressure gradient in this region is small, therefore small differences are somewhat magnified. The small differences are more evident in the surface pressure profiles shown in Figure 3.29.

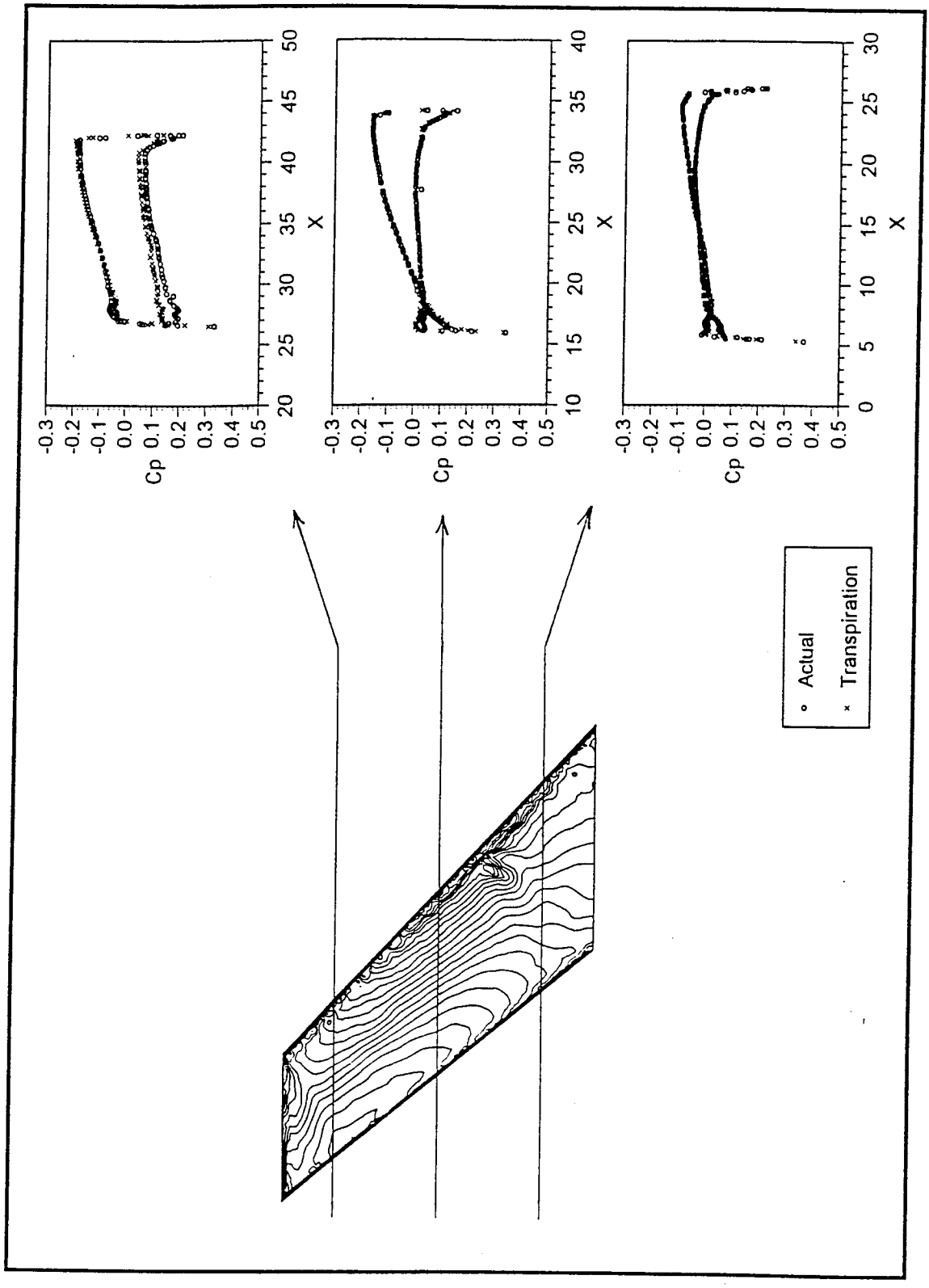

Figure 3.29. Pressure Profiles, Mach 2.0

Notice that the pressures away from the leading and trailing edges are almost identical near the root and middle of the wing. In fact, there is very good overall agreement for these two stations, with slight differences seen near the leading edge at the middle station. Again, the station near the tip shows the largest differences, as expected.

These cases clearly show that transpiration is effective at simulating even relatively large deflections in transonic and supersonic flows. Another point in the application of transpiration is in flutter studies of a severly deflected body, such as this one. Rather than using methods such as deforming meshes or transpiration to deflect the surface and perform flutter investigations, it would be simpler and possibly more accurate to perform the steady solution on the actually deflected surface, then perform the unsteady aeroelastic analysis from this solution. The deflected surface could be obtained using methods in this study, and the flutter solution could be determined with confidence using transpiration, since it is known to be accurate in simulating small disturbances.

As previously mentioned, some discussion of the sensitivity of the mesh to the flow solution is necessary so that all solution differences will not be falsely attributed to transpiration. This discussion is presented in the following section.

3.5. Mesh Sensitivity

The original plate mesh was much less refined than the one that was used to obtain the results presented in plate section. The original mesh is shown in Figure 3.30.

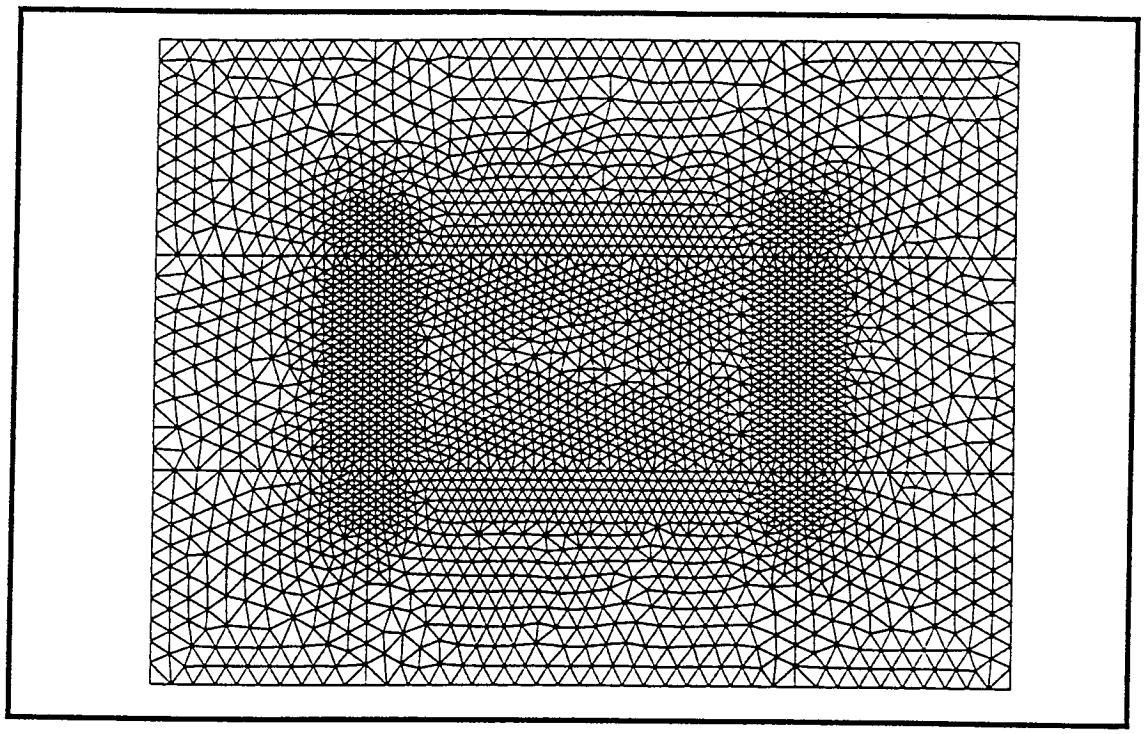

Figure 3.30. Original Plate Mesh

When observing the solutions from this original mesh, it was apparent that the elements were too small and too few to make the solution smooth. Therefore, the solution was probably somewhat inaccurate. A new mesh was constructed to produce a more accurate solution. This mesh was presented in Figure 3.4.

Pressure profiles are presented in Figure 3.31 for both the new and old actually deflected meshes for 0.1 generalized displacements at Mach 3.0.

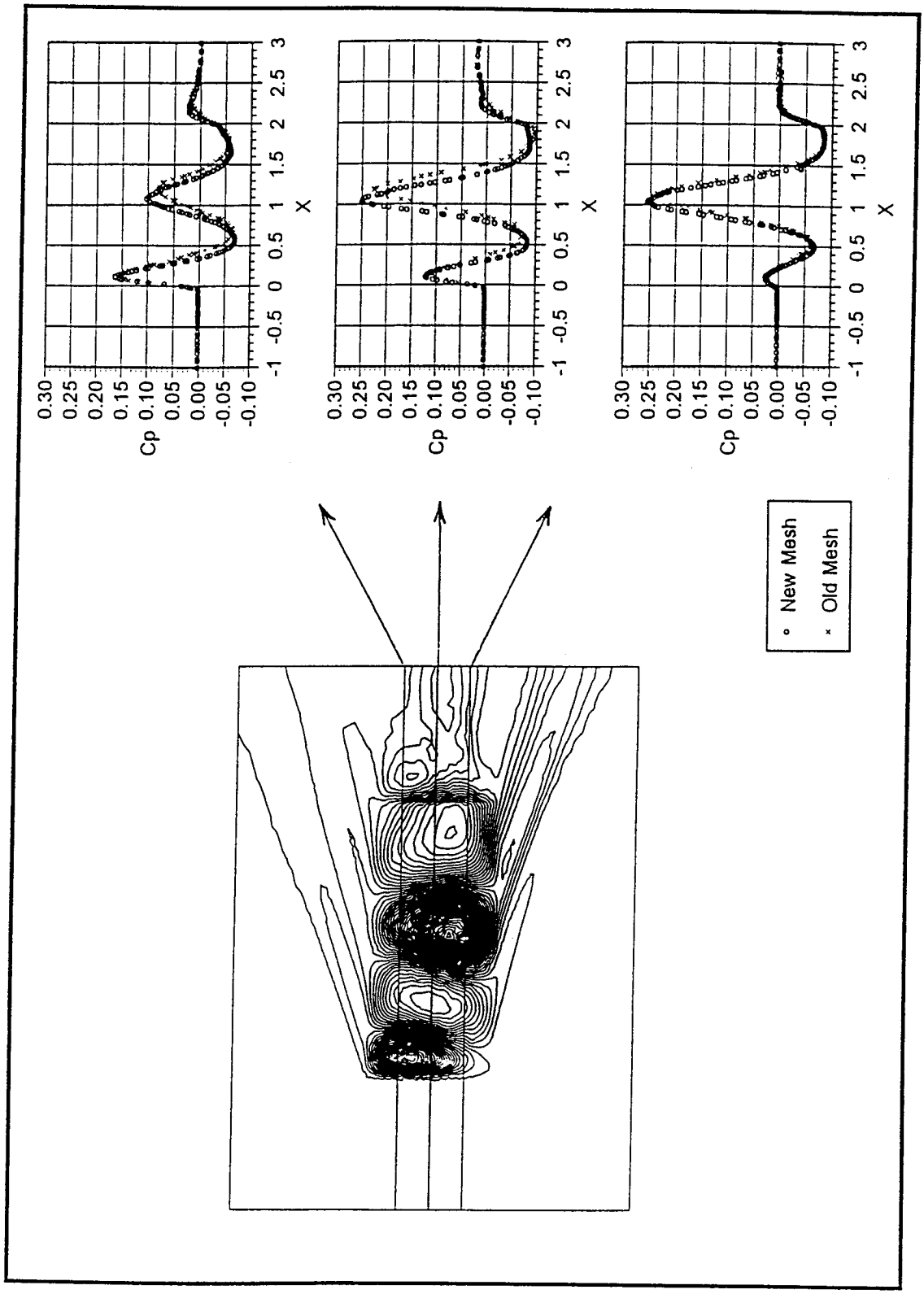

Figure 3.31. Pressure Profiles for New and Old Plate Cases

Some rather large differences are seen between the two data sets. In many areas, the differences are larger than differences that were found in the various actual and transpiration comparisons. Since the deflections and the flow conditions are the same, the difference must be the mesh.

The generalized forces that were obtained for the plate using the old mesh are presented in Table 3.4 along with the values from the new mesh (from Table 3.3).

Table 3.4. Generalized Forces for Old and New Meshes

Mode	Old Mesh	New Mesh
1	2718	2593
2	1274	534.7
3	-2564	-3708
4	-842	-848.3
5	-2872	-574.8
6	713	2248

There are significant differences in the two sets of values. Again, in some cases, the differences are larger than differences between actual and transpiration results.

Obviously, the more refined the mesh, the more accurate the solution will be. However, a more refined mesh contains more elements and nodal points, thus requiring more computational effort. The investigator must determine a balance between accuracy and practicality. Due to this mesh sensitivity, a final case was investigated where only one mesh was used to obtain comparison results. This case is presented in the following section.

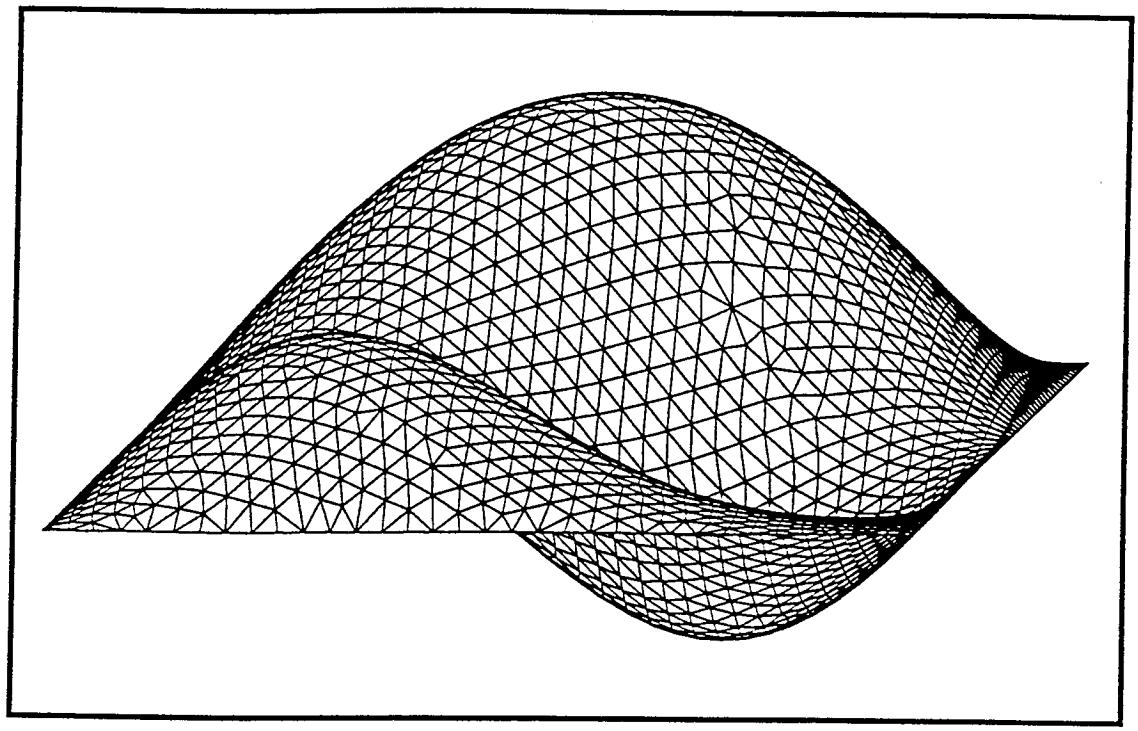

Figure 3.32. Deflected Plate, 0.5 Generalized Displacements

The remarkable amount of deflection is obvious from the figure. The deflection is so significant that it produces maximum displacement that is greater than 35% of the width. Solutions were obtained for Mach numbers 0.3, 0.8, 0.95, and 3. In each case, a well converged deflected solution was used as the starting point for the transpiration solution. In all cases, transpiration was effective in "removing" the deflection. However, results for the Mach 0.95 case were not as good as the others after the same number of iterations.

A summary of the final results for this case is given in Table 3.5.

Table 3.5. Summary of Results for 0.5 Generalized Displacement Plate

	Mach 0.3	Mach 0.8	Mach 0.95	Mach 3.0
Mach Number	0.3 ± 0.00001	0.8 ± 0.00005	0.95 ± 0.04	3.0 ± 0.001
Pressure Order of Magnitude	10^{-6}	10^{-4}	10^{-3}	10^{-6}
Average Percent Difference in GFs	2.98e-6	1.62e-5	8.27e-3	5.23e-6

From the table it can be seen that the overall Mach number becomes approximately the freestream Mach number in each case. Also, the surface pressures in each case are essentially zero with respect to their original deflected values, which were on the order of 10^{-1} to 10^{0}. The average percent error in generalized forces was calculated by averaging all of the ratios of final force value and initial force value for each mode. As an illustration of the generalized forces approach to zero, a plot of the generalized force time history for Mach 3 is presented in Figure 3.33.

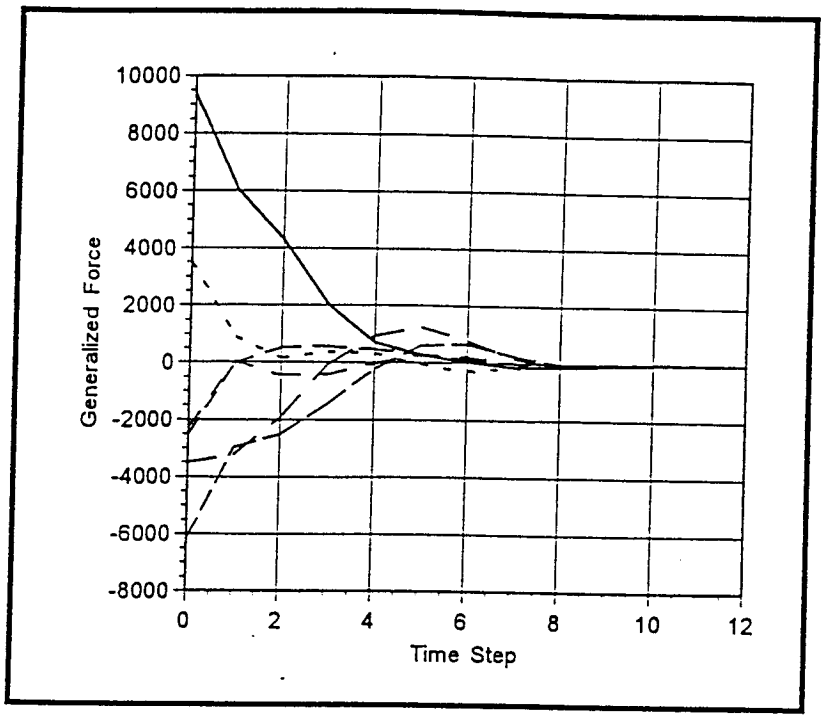

Figure 3.33. Time History of Generalized Forces

This plot is representative of the time history of generalized force for each of the other Mach numbers as well.

A plot of average percent error versus Mach number is presented in Figure 3.34.

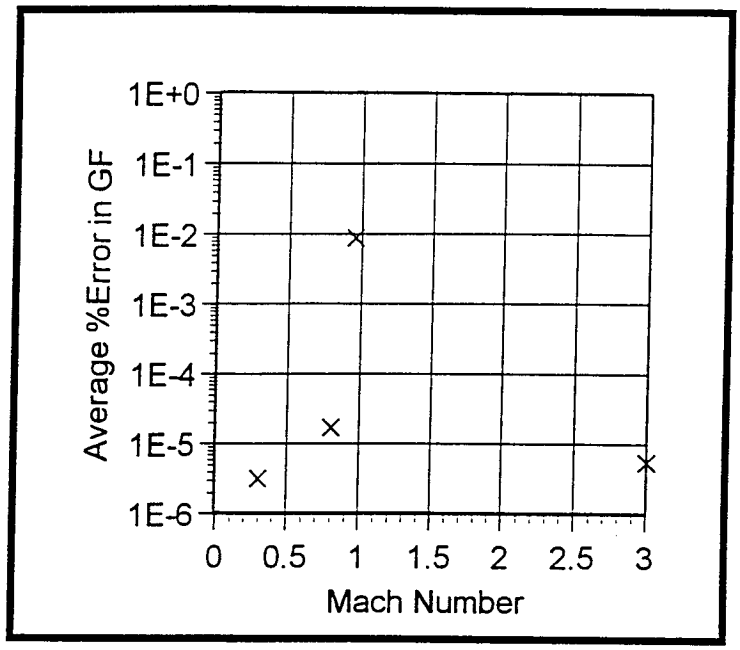

Figure 3.34. Average Percent Error in Generalized Forces

This plot suggests that transpiration was less effective in removing the deflection in the transonic range. However, since transpiration did not appear to be less effective in the other cases in the transonic range, a generalization cannot be made. Overall results for this case are very good, considering the magnitude of the deflection that is being "removed" by transpiration.

CHAPTER 4

CONCLUSIONS AND RECOMMENDATIONS

4.1. Conclusions

The primary objective of this research project was to examine the effectiveness of transpiration for simulation of structural deformations in steady and unsteady aeroelastic applications. The majority of the investigations were performed using a recently modified version of a highly integrated, finite element-based code for the multidisciplinary analysis of flight vehicles. A supplement to this code was developed in this study which allows for the generation of deflected meshes using modal superposition. This research demonstrated that the transpiration boundary condition has strong potential for applications in unsteady aeroelastic analysis, such as in the prediction of flutter boundaries. The following conclusions were reached during this investigation:

1. The transpiration boundary condition is effective in simulating even relatively large displacements over a wide range of Mach numbers. Some the results support the rationale presented for when transpiration will lose accuracy. However, there is no

strict criteria for when the transpiration boundary condition will breakdown. These results show that for applications similar to the ones presented, such as flutter prediction, transpiration can be a very effective tool in simplifying the analysis.

2. Solutions involving the application of a domain mesh can be sensitive to the refinement of the mesh. The researcher performing studies using domain meshes should investigate the sensitivity of the mesh to his or her particular application, and depending on the desired accuracy, employ the mesh that is the most practical.

3. The codes developed in this study, FROMOD and SOLMOD, can accurately and simply be used to perform surface deflections. In cases where a surface is significantly deflected from its original position before it begins to oscillate, it may be effective to use a surface deflection scheme such as this to deform the body and then perform the flutter investigation from this initial condition.

4.2. Recommendations

The cases of this study used relatively simple geometries, as compared to full body configurations. According to the transpiration concept, there should be little or no accuracy lost in using transpiration in more complex cases. However, in instances such as

intersecting shocks and surfaces, it would be interesting to see how the transpiration boundary condition performs.

Also, considering the findings on mesh sensitivity, it is recommended that any future studies using the transpiration boundary condition to compare simulated deflections with actual deflections begin with a documentation of the sensitivity of the solution to the mesh.

Finally, since the majority of these results compared computer simulations with one another, it may be advisable to compare with experimental results when available to confirm the results from the simulations.

BIBLIOGRAPHY

Anderson, D. A., Tannehill, J. C., & Pletcher, R. H. (1984). Computational Fluid Mechanics and Heat Transfer. New York: Hemisphere Publishing Corporation.

Arena, A. S. (1995-1996). Personel Communications.

Batina, J. T. (1989). Unsteady Euler Airfoil Solutions Using Unstructured Dynamic Meshes. AIAA Paper 89-0115, American Institute of Aeronautics and Astronautics.

Bharadvaj, B. K. (1990). Computation of Steady and Unsteady Control Surface Loads in Transonic Flow. AIAA Paper 90-0935, American Institute of Aeronautics and Astronautics.

Dixon, S. C. (No date given). Comparison of Panel Flutter Results from Approximate Aerodynamic Theory with Results from Exact Inviscid Theory and Experiment, NASA TN D-3649.

Gupta, K. K. (1995). An Integrated, Multidisciplinary Finite Element Structural, Fluids, Aeroelastic, and Aeroservoelastic Analysis Computer Program. Edwards, CA: National Aeronautics and Space Administration.

Henne, P. A. (1990). Applied Computational Aerodynamics. Washington, DC: American Institute of Aeronautics and Astronautics, Inc.

Lighthill, M. J. (1958). On Displacement Thickness. Journal of Fluid Mechanics, 4(4), 383-392.

Malone, J. B. & Sankar, L. N. (1985). Unsteady Full Potential Calculations for Complex Wing-Body Configurations. AIAA Paper 85-4062, American Institute of Aeronautics and Astronautics.

Malone, J. B., & Sotomayer, W. A. (1984). Unsteady Aerodynamic Modeling of a Fighter Wing in Transonic Flow. AIAA Paper 84-1566, American Institute of Aeronautics and Astronautics.

Raj, P., & Harris, B. (1993). Using Surface Transpiration with an Euler Method for Cost-Effective Aerodynamic Analysis. AIAA Paper 93-3506, American Institute of Aeronautics and Astronautics.

Ruo, S. Y., & Sankar, L. N. (1988). Euler Calculations for Wing-Alone Configuration. Journal of Aircraft, 25(5), 436-441.

Sankar, L. N., Malone, J. B., & Schuster, D. (1987). Euler Solutions for Transonic Flow Past a Fighter Wing. Journal of Aircraft, 24(1), 10-16.

Sankar, L. N., Malone, J. B., & Tassa, Y. (1981). An Implicit Conservative Algorithm for Steady and Unsteady Three-Dimensional Transonic Potential Flows. AIAA Paper 81-1016, American Institute of Aeronautics and Astronautics.

Sankar, L. N., Ruo, S. Y., & Malone, J. B. (1986). Application of Surface Transpiration in computational aerodynamics. AIAA Paper 86-0511, American Institute of Aeronautics and Astronautics.

Thomson, W. T. (1988). Theory of Vibration with Applications (3rd ed.). New Jersey: Prentice Hall.

SECTION II

ALTERNATIVE SUPERSONIC AERODYNAMIC PREDICTION METHODOLOGY STUDY

TABLE OF CONTENTS

NOMENCLATURE

a_∞, P_∞, ρ_∞, M_∞	= velocity of sound, pressure, density, and mach number respectively, in free stream conditions
a_o, P_o, ρ_o, M_o	= velocity of sound, pressure, density, and mach number respectively, in mean flow
C_p	= coefficient of pressure
C_L	= coefficient of lift
γ	= 1.4, ratio of specific heats
δ	= impact angle with free-stream velocity
θ_o	= mean flow angle
θ'	= perturbed angle
M_{ns}	= mach number normal to shock
$\mathbf{n}$	= outward normal
$\mathbf{n}'$	= outward normal perturbed from mean flow
P	= Pressure
P′	= pressure perturbed from mean flow
q	= generalized displacement
w(t)	= piston velocity as a function of time
V_b	= velocity of body
V_s	= local steady velocity

1. INTRODUCTION

A prediction of aircraft flight dynamics and aeroelastic characteristics such as flutter[1] are crucial to the design of modern aircraft as well as to flight test operations. Recently, there has been resurgent interest in the development of hypersonic vehicles which operate in speeds where flutter may occur during at least part of the vehicle's operation. Examples of such vehicles include the Space Shuttle, Pegasus, the National Aerospace Plane (NASP), and the X-34. Also presently under development is the X-33, which is a joint effort between NASA and major aerospace companies, and will be the world's first single stage to orbit vehicle.

Using a recently developed STARS[2] capability for aeroelastic analysis, a time-marching approach based on the unsteady Euler equations may be utilized to predict flutter boundaries over a wide Mach number range for complex three-dimensional geometries. Determination of the flutter boundaries is presently achieved by searching over the flight regime for potential crossovers between stable and divergent time history oscillations based on modal damping terms. This analysis is followed by interpolation of these results to determine the point at which the system is neutrally stable.

STARS which stands for "Structural Analysis RoutineS" was developed by Gupta[2] at the NASA Dryden Flight Research Center. STARS is a highly integrated code for multidisciplinary analysis of flight vehicles including static and dynamic structural analysis, computational fluid dynamics, heat transfer, and aeroservoelasticity capabilities. With the recently developed capability for Aeroelastic analysis using a time-marching approach based on the unsteady Euler equations, the aforementioned prediction of flutter boundaries may be obtained for a wide variety of flight conditions and geometries.

Due to the potentially large domain required to ensure sufficient grid resolution of a given geometry, however, there lies a critical drawback of the time-marching approach. Dowell[3] points out that the computational time required will be on the order of $\mathbf{P} * \mathbf{T_F}$ where $\mathbf{P}$ is the number of parameter combinations required and $\mathbf{T_F}$ is the time required for a simultaneous fluid-structure time marching calculation to complete a transient. In order to ensure time accuracy and sufficient grid resolution, the use of time-marching solutions to the Euler equations on a three-dimensional configuration requires a significant amount of computation time. As an illustration, on a present day high speed workstation, utilization of the unsteady Euler equations to calculate a single fluid structure transient on a three-dimensional system may demand well in excess of one-hundred CPU hours. Hence, identification of the flutter boundaries over the full domain will require many times this number.

2. FOCUS OF THE PRESENT INVESTIGATION

The focus of the present investigation is to enhance the practicality of the time-marching aeroelastic analysis by combining aerodynamic modeling techniques and Computational Fluid Dynamics in order to significantly reduce the computational time required for an aerodynamic solution of a given geometry in the supersonic flight regime. Moreover, the error of such a method must be well within acceptable limits as compared with experimental data or the predictions of the unsteady Euler equations previously discussed.

3. METHODS CONSIDERED

Since it is the CFD which requires the overwhelming proportion of the computation time, a method which gives an accurate estimate to later be refined is researched. Different areas of importance in the determination of such a method are as follows: Since this procedure will be implemented into STARS, ease of implementation and compatibility must be considered. Also, this method must be accurate over a wide range of geometric shapes and flow regimes, and not just limited to special cases. Simplicity is also a plus, hence a basic method would augment ease of rigorous testing and validation over the widest range possible. Different methods with these goals in mind are discussed.

3.1. Piston Method

The piston method[4] is a popular technique for supersonic and hypersonic flutter prediction. In the form of the unsteady wave equation, this method requires only the outward normal vector on a given surface to determine the pressure at any point. Figure 3-1 illustrates the unsteady wave equation is as follows:

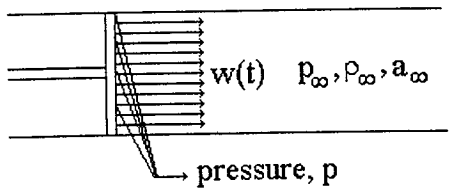

Figure 3-1 Piston motion in a one-dimensional channel.

where: $$p = p_\infty \left[1 + \frac{\gamma - 1}{2} \frac{w}{a_\infty}\right]^{\frac{2\gamma}{\gamma - 1}} .$$

Due to its simplicity and ease of use, it is an attractive technique for approximating the surface pressure in a supersonic flow. The unsteady wave equation, however, does not take into account the losses across a shock nor does it accurately predict pressure in a shock interaction area. Furthermore, since this theory is based on a point function, i.e., the pressures are only dependent upon local conditions, it over predicts the pressure on a three-dimensional geometry such as a cone. This is due to the three-dimensional relaxing effect for which the piston theory cannot account. Also, for a relatively blunt surface with respect to the flow, the piston method again over predicts the pressure. As an example, in figure 3-2, the unsteady wave equation is used to show the pressure coefficient versus mach number for a wedge and a cone at half angles of ten degrees. Since the piston theory does not differentiate between the two geometries and is based on the assumption that the flow is a point function, only one curve represents both geometries. This curve is compared with data taken from literature for a cone[5] and wedge[6] at the noted half angle.

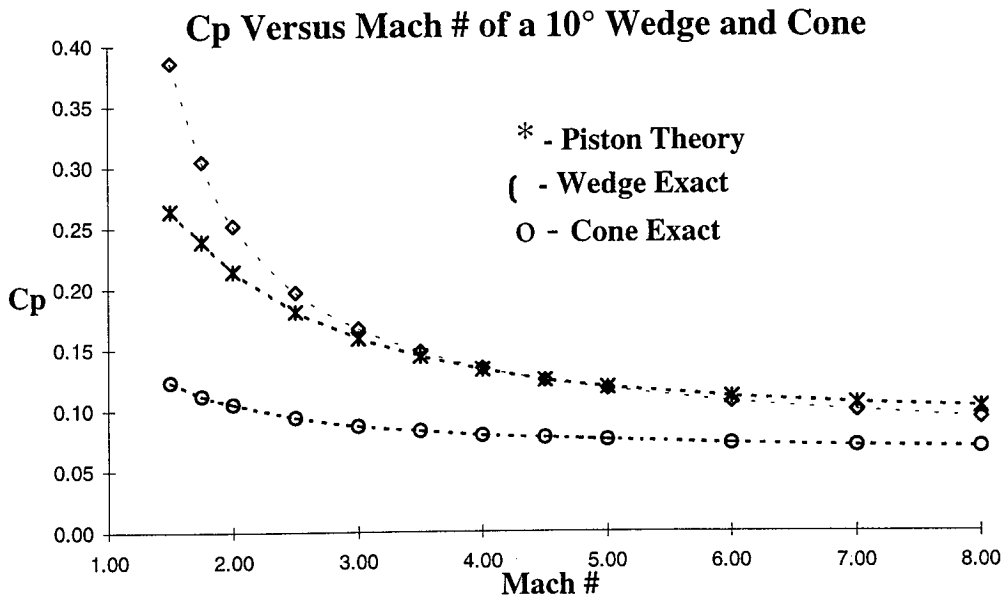

Figure 3-2 Pressure coefficient versus Mach number for a wedge and cone at half angles of ten degrees as applied to Piston Theory.

Figure 3-3 shows the percent error of the application of Piston theory to both the wedge and a cone as compared with data from the literature.

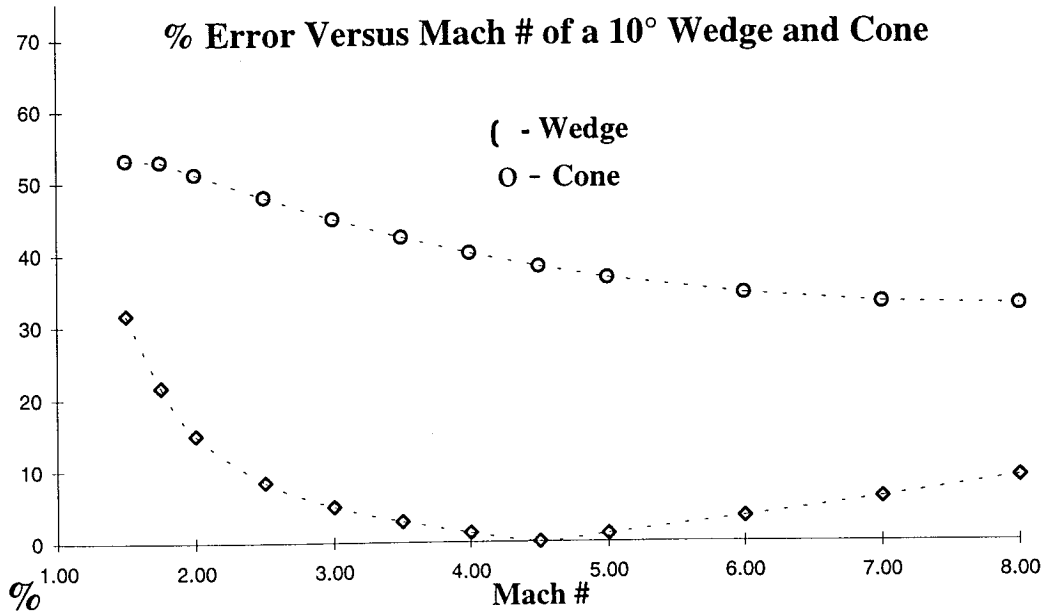

Figure 3-3 Percent error of Piston theory application to the wedge and cone.

Clearly the unsteady wave equation predicts pressure well over a predominately two dimensional flow surface yet over predicts pressure on a more three-dimensional flow surface such as the cone with the same half angle.

Due to the limited application range and accurate prediction of pressure via the Piston theory, a method which will better predict surface pressure about a more three-dimensional flow is considered.

3.2. Tangent-Cone Method

The Tangent-Cone[7] method is an approximate technique for the prediction of three dimensional pressure effects on a cone surface analogous to the nose of a fuselage for example. The equations for the surface pressure are as follows:

$$C_p = \frac{48 \cdot M_{ns}^2 \cdot \sin^2 \delta}{23 \cdot M_{ns}^2 - 5}$$

where: $$M_{ns} = \left(0.87 \cdot M_\infty - 0.544\right) \cdot \sin \delta + 0.53$$

C_p is based on the Modified Newtonian[8] theory which yields a result as a function only of the impact angle δ:

$$C_p = K \cdot \sin^2 \delta$$

Here K[8] is equal to the stagnation pressure coefficient and M_{ns} is the mach number normal to the shock which is empirically determined by Edwards[9]. Results and further explanation of this method may be found in reference 8.

The Tangent-Cone method under predicts pressure for predominately two-dimensional flow and again over predicts pressure for flows about blunt surfaces such as the leading edge of a wing. Furthermore, as in the Piston Method, the Tangent-Cone method neglects the effects of the mean flow and any shock interactions.

3.3. Modified Newtonian Impact Method

In contrast to the unsteady wave equation and the Tangent-Cone procedure, the Modified Newtonian Impact[8] method is used predominately for very blunt surfaces relative to the free-stream flow or at very high mach numbers in the hypersonic range. The equation for the Modified Newtonian Impact theory is previously discussed with the Tangent-Cone method and is also listed as follows:

$$C_p = K \cdot \sin^2 \delta$$

For true Newtonian flow, the parameter K is given as 2, and for the Modified theory, K is taken as the stagnation C_p.

Since however, this method has a limited application of mainly blunt surfaces at high supersonic to hypersonic speeds, other methods are again considered.

4. Other Methods

There are a number of other methods for prediction of surface pressure in supersonic and hypersonic flow. The Modified Newtonian Plus Prandtl-Meyer Method for example is another blunt body technique based on the analysis presented by Kaufman[8]. Or even the Van Dyke Unified Method[8] useful for thin profile shapes. These methods are usually applied to specific cases and tend to be too specific for the task at hand.

5. METHODOLOGY

After careful examination and analysis of several different methods to augment the efficacy of the STARS code in flutter boundary prediction, the Piston method is chosen not only to be implemented into to STARS but also to be utilized as a perturbation to an already existing mean flow solution, hence the Piston Perturbation Method. A brief illustration of this idea, utilizing a cone similar to the one used for the generation of figure 3-3, is shown in figure 5-1 where the unsteady wave equation is modified to predict the pressure for a perturbations about the mean flow from 10° to 12.5°. The modified unsteady wave equation is as follows:

$$\frac{P'}{P_\infty} = \frac{P_o}{P_\infty}\left[1+\frac{\gamma-1}{2}M_o Sin(\theta'-\theta_o)\right]^{\frac{2\gamma}{\gamma-1}}$$

where figure 5-1 illustrates this equation.

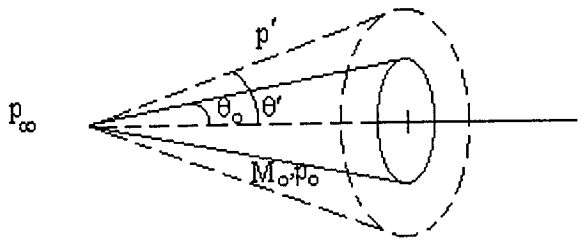

Figure 5-1 An illustration depicting the modified unsteady wave equation for a cone.

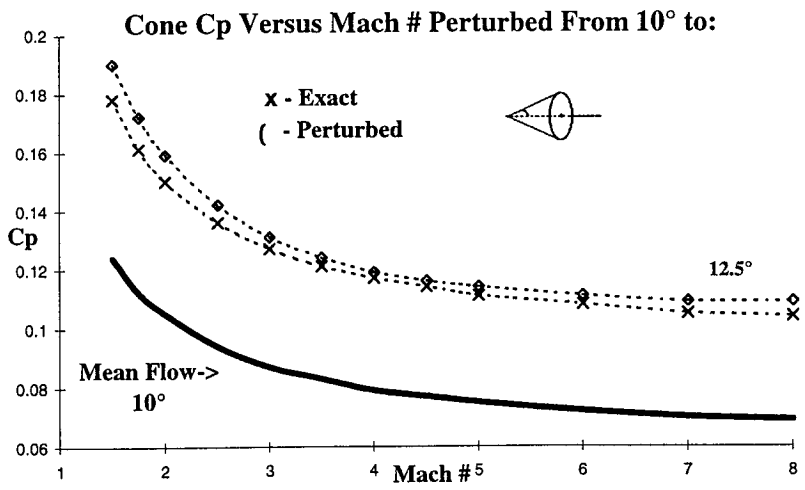

Figure 5-2 Pressure coefficient of a cone perturbed about the mean flow of 10° to 12.5°.

Previously in figure 3-2, Piston theory was applied to a cone without taking into account the mean flow conditions. Figure 5-3 shows the percent error of figure 5-2, which comparatively shows better results than the previous situation.

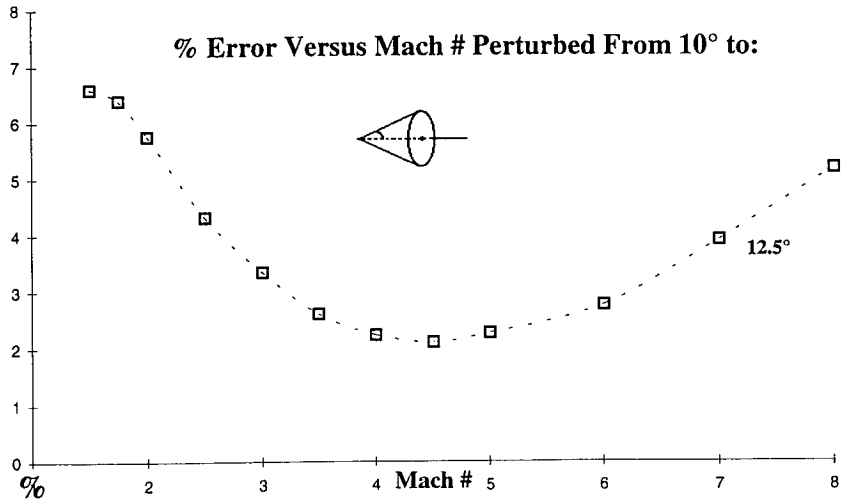

Figure 5-3 Percent error versus Mach number for Cp of a cone perturbed from 10° to 12.5°.

Clearly, the percent error is less for the perturbed case than the unperturbed case in figure 3-3.

The Perturbation method has been implemented in STARS in the following manner: Initially, a supersonic steady-state solution for a three-dimensional flow field is obtained with the use of the finite-element Euler methodology. The flow variables, which take into account the non-linearities due to three-dimensional effects such as shock interactions, are saved and used as a mean flow to the starting point of the aeroelastic simulation. Once these variables are obtained, they may be saved and used for future simulations given the structure is not significantly altered. With the steady state Euler solution given as the mean flow, modal superposition is applied in the simulated aerodynamic structure to represent the aeroelastic effects. The modes of vibration are perturbed which represents a perturbation to the mean flow. Next, an application of the isentropic wave equation previously discussed is locally applied as a perturbation to the mean flow at every point. The equations governing this method are shown here with figure 5-4:

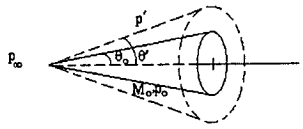

Figure 5-4 Simplistic illustration of a locally applied perturbation to the mean flow.

where:
$$\frac{P'}{P_\infty} = \frac{P_o}{P_\infty}\left[1 + \frac{\gamma - 1}{2}\frac{V_\infty \Delta u^*}{a_o}\right]^{\frac{2\gamma}{\gamma-1}}$$

and in non-dimensional form:
$$\frac{P'}{P_\infty} = \frac{P_o}{P_\infty}\left[1 + \frac{\gamma - 1}{2} M_\infty \frac{a_\infty}{a_o}\Delta u^*\right]^{\frac{2\gamma}{\gamma-1}}$$

with: $$\frac{a_\infty}{a_o} = \sqrt{\frac{P_\infty / \rho_\infty}{P_o / \rho_o}}$$

and $$\Delta u^* = V_s \cdot n' + V_b \cdot n'.$$

These pressures are then used in the coupled structural dynamic solutions which are numerically integrated to find a generalized displacement q shown as:

$$[M] \cdot \ddot{q} + [K] \cdot q = [P]$$

where [M] and [K] are the mass matrix, and the stiffness matrix respectively, obtained in STARS by a finite element structural analysis routine given the structural properties of the system and [P] is the force matrix obtained by the piston perturbation method. Once the generalized displacement for every point on the aeroelastic surface is determined, the values are multiplied by the mode shapes to determine the actual displacement for calculation of a new set of transient data.

Given the new structural deflections based on the previous aerodynamic pressures, a new outward normal velocity is given for the next calculation of the pressures. This process repeats until enough transient data is acquired to determine the stability characteristics of the perturbed aerodynamic system. Finally, the flutter boundaries are then verified and refined with the non-linear time marching Euler method.

6. RESULTS

It will be shown that the Piston Perturbation method accurately predicts surface pressure of a number of different geometrical configurations in the supersonic flow region. It will also be shown that the estimated flutter boundaries of a Generic Hypersonic Vehicle (GHV) obtained by this method are sufficiently close to the flutter boundaries obtained by the Euler method, that the estimated CFD solution may then be used for refinement which requires significantly fewer transient calculations. This GHV will also be used to compare predicted flutter boundaries, and run time between the perturbation solution and the Euler solution.

To show the simplicity and accuracy of the piston perturbation solution, a simple perturbed wedge exemplifies the validly of this method over a wide range of mach numbers for perturbations about the mean flow. Figure 6-1 shows these results.

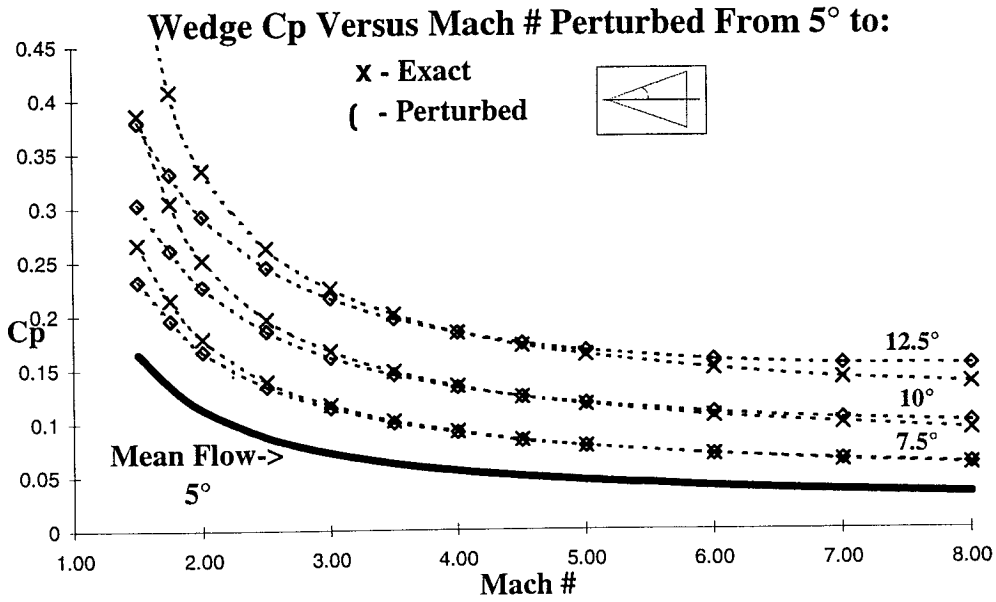

Figure 6-1 A simple perturbed wedge in compression.

The Perturbation method also predicts pressure for an expansive perturbation as shown in figure 6-2.

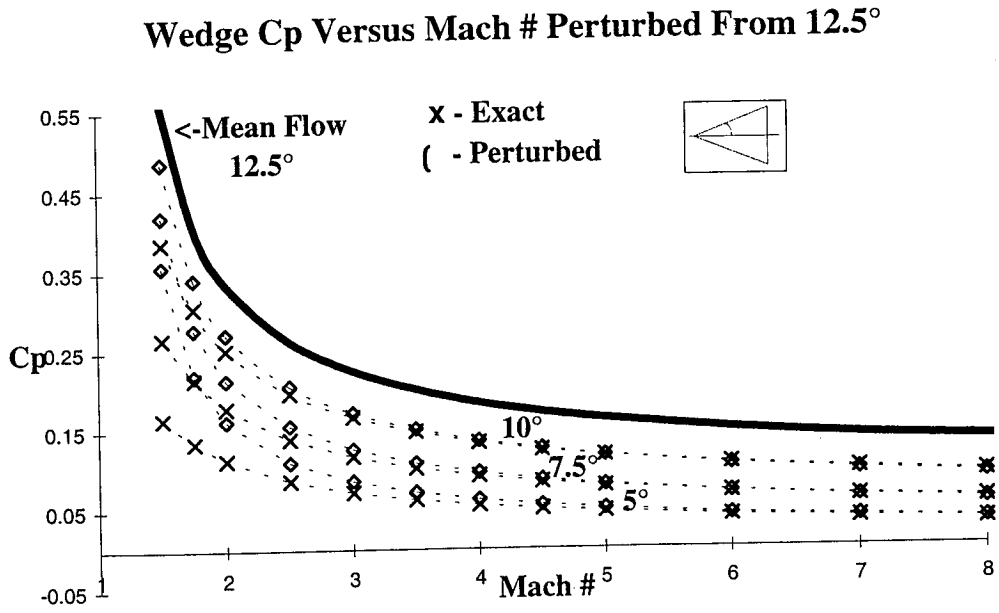

Figure 6-2 A simple perturbed wedge in expansion.

The errors are minimal given a perturbation approximately less than 30% of the mean flow conditions and w/a_o between -1 and +1 where negative and positive values represent expansion and compression respectively. The term w/a_o is similar to w/a_∞[10] in the unsteady wave equation previously noted except it is perturbed about the mean flow not the free stream. Since the majority of flutter analyses deals mostly with small perturbations this criteria holds for a wide range of mach numbers and geometries.

The P.S. also predicts pressure about more three dimensional surfaces, such as cones, over a wide range of mach of mach numbers in compression as well as in expansion shown in figures 6-3, and 6-4 as follows.

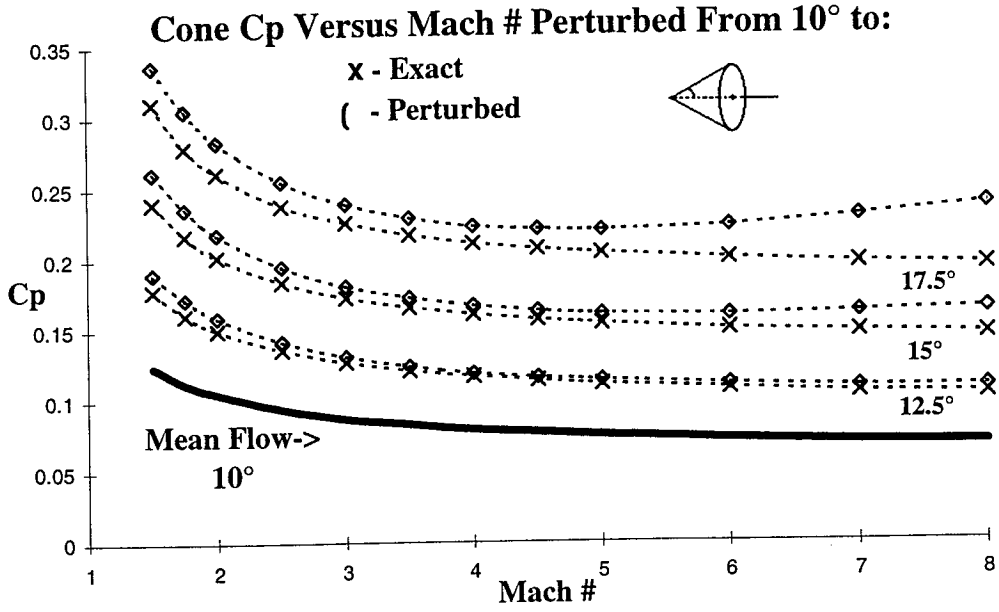

Figure 6-3 A simple perturbed cone in compression.

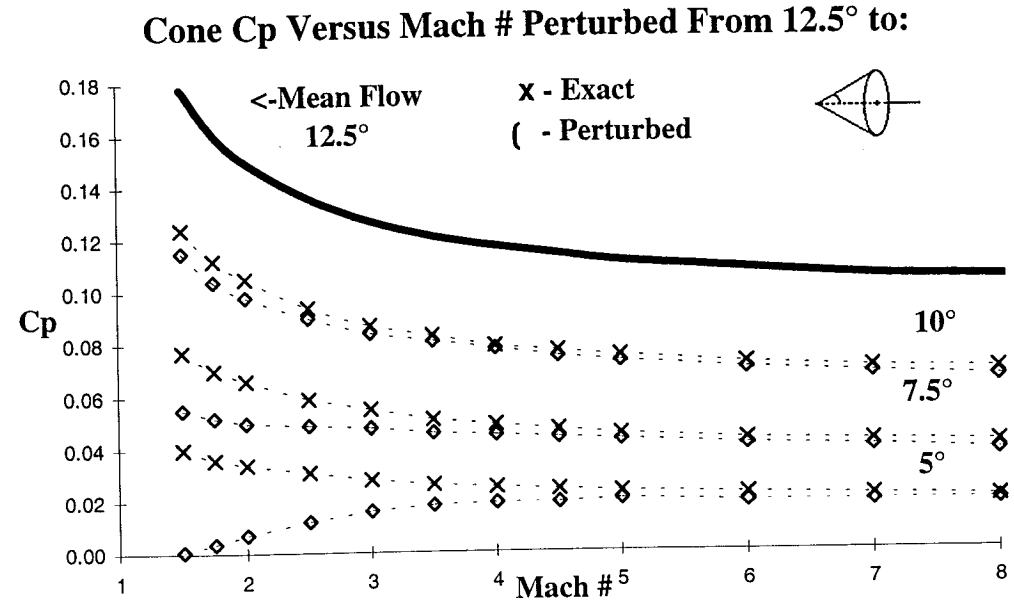

Figure 6-4 A simple perturbed cone in expansion.

Again, the P.S gives accurate results, in the reasonable situations, of the surface pressure since it is applied as a small perturbation to the mean flow where the three-dimensional relaxation effects are accounted for.

Another advantage of the Perturbation method is it's ability to capture pressure predictions when nonlinearities such as shock interactions exist in the mean flow. As shown in the following image (figure 6-5), at $M_\infty = 2.2$, a shock induced by a rigid wedge in a fixed rectangular duct interacts with an elastic clamped flat plate with differential pressure on the outer part of the duct.

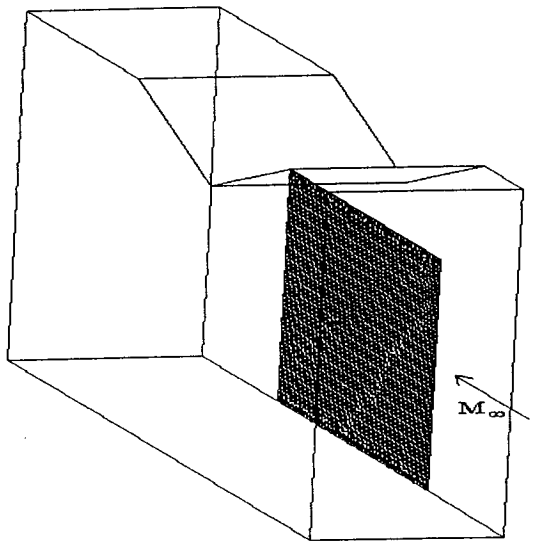

Figure 6-5 A fixed rectangular duct with an elastically flexible clamped flat plate.

A side view of this geometry (figure 6-6) shows the pressure contours generated by steady Euler equations. Notice the heavy shock interactions due to the wedge and rigid boundaries of the geometry.

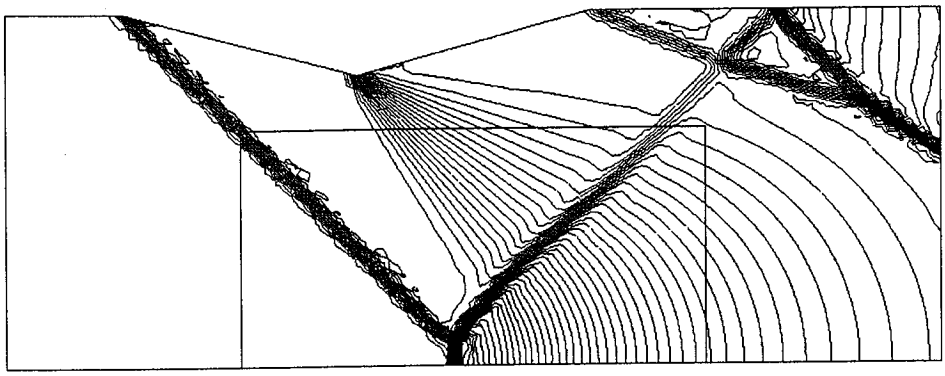

Figure 6-6 A side view showing the pressure contours of the heavy shock interactions with the elastic plate.

A magnified view for the steady state deformation of the elastic plate generated by the unsteady Euler equations is shown in figure 6-7.

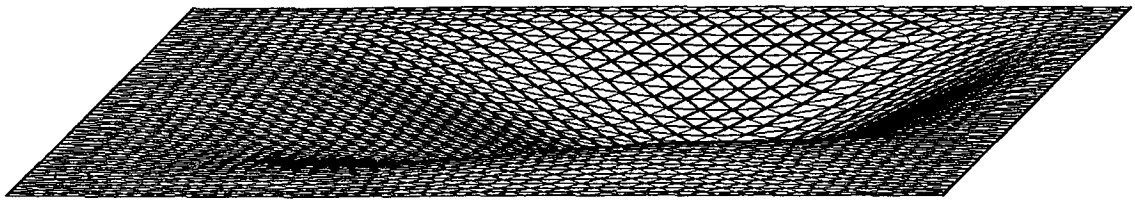

Figure 6-7 Steady state deformation of the elastic plate generated by the unsteady Euler equations.

This deformation was generated by first running a steady Euler solution to obtain the aerodynamic properties throughout the duct. Next, the process is restarted, this time allowing the plate to deform due to the resulting aerodynamic forces just acquired. After the plate's oscillation damps out, steady state deflection is achieved. Notice the plate's outward deformation due to the shock induced by the rigid wedge.

As a comparison, pressure using the piston theory is calculated and shown below in figure 6-8.

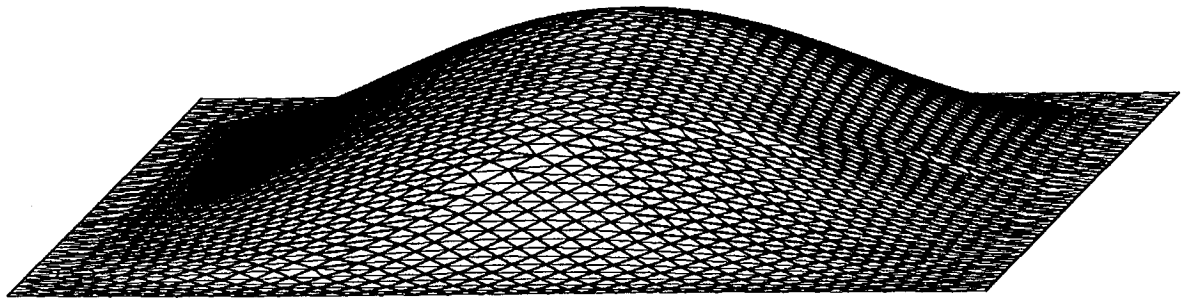

Figure 6-8 Steady state deformation of the elastic plate generated by piston theory.

Since this theory only takes into account the local conditions, the pressure induced by the shock is totally neglected causing large error in the prediction of the steady state deformation. The Perturbation solution is now applied with the following results in figure 6-9.

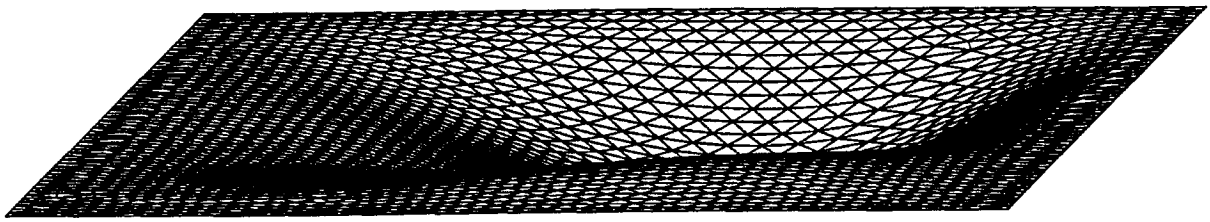

Figure 6-9 Steady state deformation of the elastic plate generated by the Perturbation method.

Since the perturbation method perturbs about the mean flow, the pressure induced by the shock is accounted for giving more accurate results as compared with the Euler steady state deformation in figure 6-7 above.

As another example of the capability of the Perturbation method, the pressure at three sectional cuts on a Generic Hypersonic Vehicle (GHV) at Mach 2.2 is calculated at a 5° angle of attack using the P.S. The piston method, and a steady Euler solution is also calculated for comparison. For the perturbation method, the GHV is perturbed 1° about a steady Euler solution at 4° with the following results shown in figure 6-10.

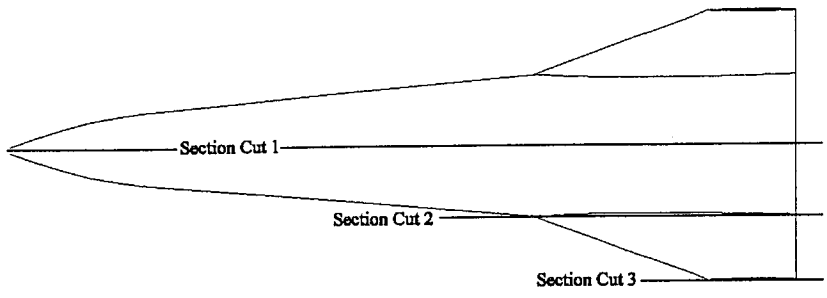

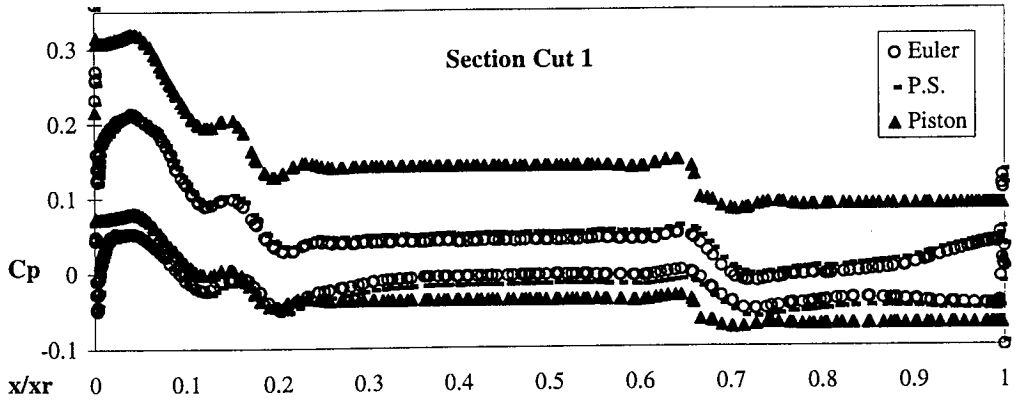

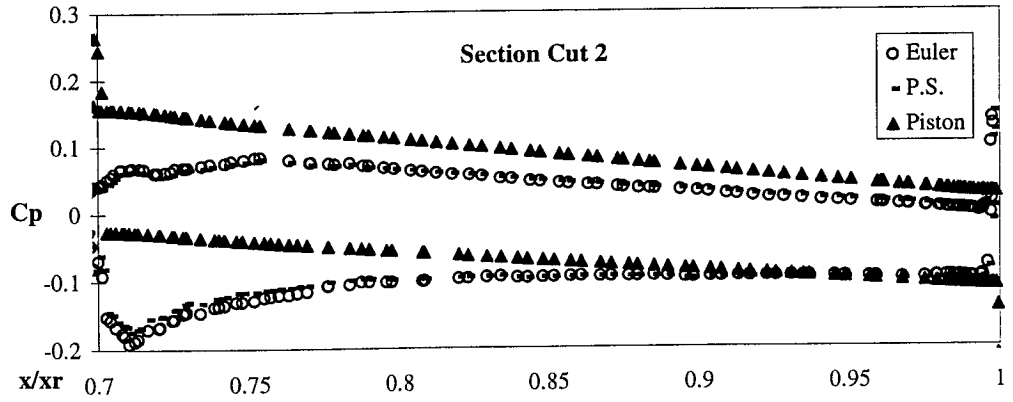

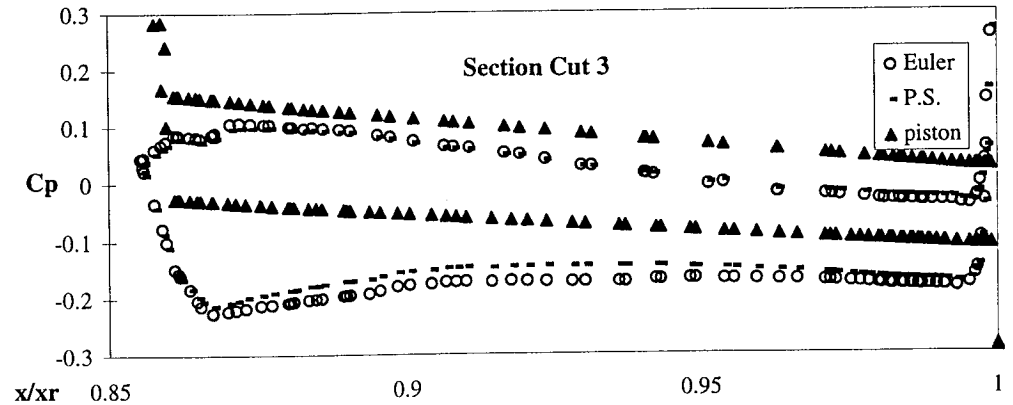

Figure 6-10 Pressure comparisons at 5° angle of attack using Euler, Piston, and Perturbation method at three sectional cuts on a GHV.

As another illustration of the perturbation method a surface mesh of the baseline configuration for the GHV is generated (fig. 6-11).

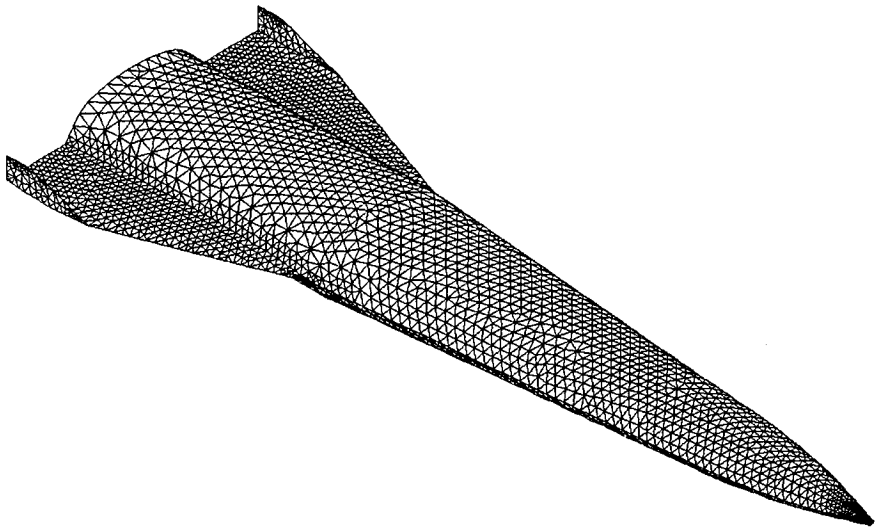

Figure 6-11 GHV Baseline surface Mesh

Flutter analysis is then performed in the following manner: Given the surface mesh, a finite-element structural model is then developed to obtain the structural mode shapes and frequencies. Details of this structural modeling may be found in references 2,11, and 12. Next, a steady solution to the flow field at Mach 2.2 was obtained using the finite-element Euler methodology which is used as the mean flow condition about which the perturbation solution is applied. The aeroelastic simulation consists of a 9 mode solution for 705 time steps (which is approximately 7 cycles of mode 1). The Euler solver is run over a range of 4 dynamic pressures, and the flutter boundary is estimated through polynomial interpolation. For the purpose of run-time comparison, the same procedure is used for the perturbation solution.

As seen in Figure 6-12, the difference among flutter boundary estimates between the two codes for this case is found to be less than 4%, however the difference in run times is extremely significant.

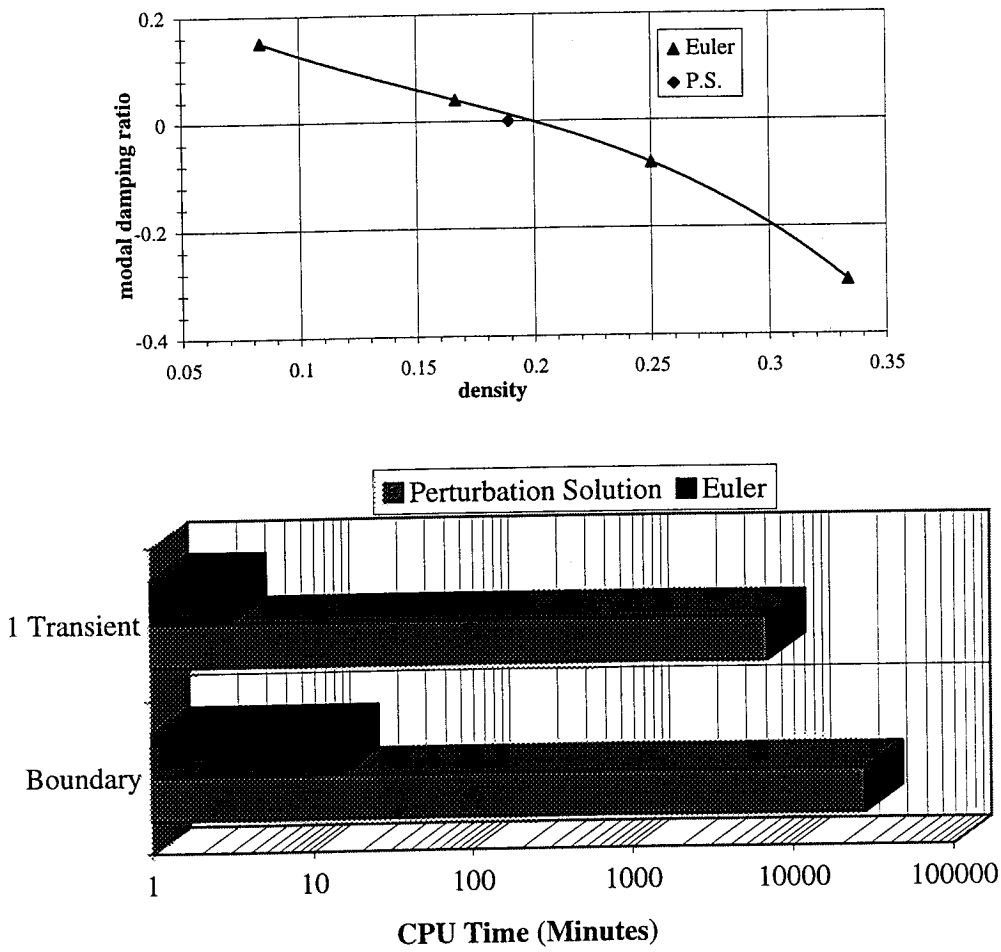

Figure 6-12 Flutter boundary and run-time comparisons.

M=2.2, 705 time steps / transient

Run time for the perturbation solution (P.S.) estimate is 3 minutes for each transient or approximately 15 minutes to identify the flutter boundary. On the other hand, run time for the Euler solution used to define the flutter boundary is 117 hours for each transient and

approximately 469 hours to identify the boundary. All simulations are run on an IBM RS6000 3BT workstation.

As a final illustration of the perturbation method, the following geometry is considered to examine the flow characteristics about a three dimensional flow field in which a highly three dimensional flowfield interacts with a swept wing.. The analysis is conducted in a manner similar to that used for the GHV case. The baseline geometry may be seen in figure 6-13.

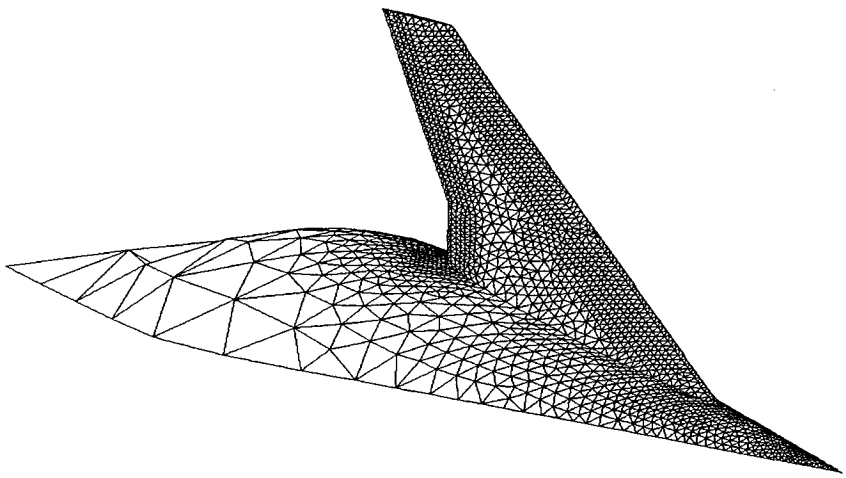

Figure 6-13 Test case baseline mesh.

A wing with a biconvex cross section is swept 42 degrees which makes the design Mach number when placed on the 15° cone approximately 1.6. Since steep gradients require a fine mesh which requires more computation time, the cone is tapered aft of the swept wing. Since the taper is gradual and the flow is supersonic (flow effects may not propagate forward), this area may be coarsely meshed aiding in computational efficiency. Mach 1.6 is one Mach number considered along with Mach 1.3 and Mach 2.4. Figure 6-14 shows the pressure contours at mach 1.6 of this configuration.

Figure 6-14 Pressure contours at Mach 1.6

The perturbation method and the Piston method are used to determine the flutter boundary at Mach 1.6. Next, these boundaries are compared with the flutter boundary determined by the unsteady Euler equations. Comparisons of analyses show a less than 5% error in the prediction of the flutter boundary between the perturbation solution and the Euler solution. The piston-only solution is in error by 37.5%

The same analysis is performed at mach 2.4. Note how the shock produced by the cone interacts with the wing at about mid-span (fig. 6-15). This is a typical example where the Perturbation method is able to predict three-dimensional flow characteristics by accounting for the nonlinearities and three-dimensional effects in the mean flow. A plot of the steady-state pressure contours used as the mean flow conditions for the P.S. is shown in figure 6-15.

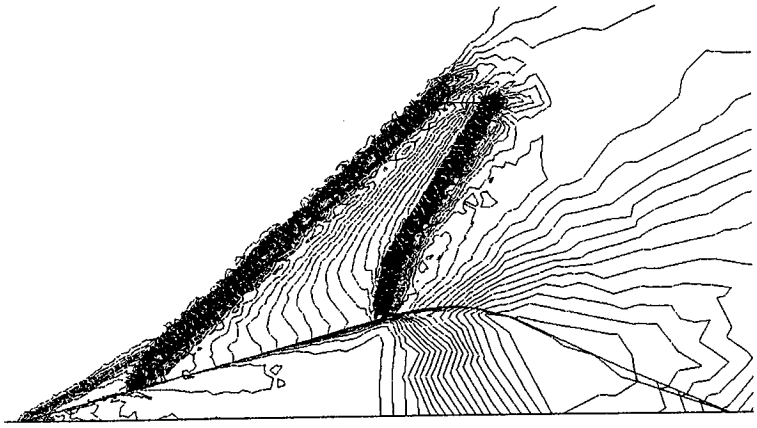

Figure 6-15 Pressure contours at Mach 2.4.

Flutter prediction results are again similar to those seen at other Mach numbers. Differences between the perturbation solution and the Euler solver are again less than 5%, while the piston-only solution is in error by 20%.

7. CONCLUSIONS

Obtained results reveal that the combination of aerodynamic modeling with CFD methodology enhance the practicality of the use of time-marching CFD for supersonic aeroelastic calculations in an operational environment. This method was tested over a wide range of mach numbers and proven valid in all reasonable cases. Furthermore, the application of this method in areas of shock interactions was studied and also proven accurate. It was shown for the configurations tested that the time required to predict flutter by time marching CFD can significantly be reduced by first obtaining an accurate estimate using modeling techniques. Furthermore, present research also indicates significant time savings in the identification of critical flight conditions for aircraft-type configurations in addition to the ones discussed here. It

was demonstrated that for highly-three dimensional configurations, and for configurations for which significant nonlinearities exist in the mean flow, the perturbation method developed, is superior to methods which cannot account for the mean flow.

An added advantage of the presented approach is that the same grid may be used for the steady CFD solution, the perturbation model, and the time marching CFD solution. In addition, the method used can be easily implemented in any CFD algorithm capable of simulating supersonic flow fields with relatively minimal increase in code size and complexity.

8. REFERENCES

[1]Fung, Y. C., "An Introduction to the Theory of Aeroelasticity", 1st edition, Dover Publishers, 1969.

[2]Gupta, K.K., "STARS - An Integrated General-Purpose Finite element Structural, Aeroelastic, and Aeroservoelastic Analysis Computer Program," NASA TM-101709, Jun. 1990.

[3]Dowel, E.H., Crawley, E.F., Curtiss, Jr., H.C., Peters, D.A., Scanlan, R.H. and Sisto, F., "A Modern course in Aeroelasticity", 3rd edition, Klewer Academic Publishers, 1995.

[4]Holt, Ashley, Zartarian, Garabed. "Piston Theory-A New Aerodynamic Tool for the Aeroelastician", presented at the Twenty-Forth Annual Aeroelasticity Meeting, January, 1956.

[5]Sims, Joseph L., "Tables for Supersonic Flow Around Right Circular Cones at Zero angle of Attack", NASA SP-3004, 1964.

[6]Neice, Mary M., "Tables and Charts of Flow Parameters Across Oblique Shocks", NACA TN 1673, August, 1948.

[7]Cruz, Christopher I., Sova Gregory J., "Improved Tangent-cone Method for the Aerodynamic Preliminary Analysis System (APAS) Version of the Hypersonic Arbitrary-Body Program", NASA TM 4165, February, 1990.

[8]Bonner, W. E., Cleaver, K. Dunn, "Aerodynamic Preliminary Analysis System II. Part I Theory", NASA CR-165627, 1981.

[9]Pittman, Jimmy L. (appendix by C. L. W. Edwards): "Application of Supersonic Linear Theory and Hypersonic Impact Methods to Three Nonslender Hypersonic airplane Concepts at Mach Numbers From 1.10 to 2.86". NASA TP-1539, 1979.

[10]Lighthill, M. J., "Oscillating Airfoils at High Mach Number", Journal of the Aeronautical Sciences, vol. 20, No. 6, pp. 402-406, June, 1953.

[11]Gupta, K.K., Peterson, K., and Lawson, C., "Multidisciplinary Modeling and Simulation of a Generic Hypersonic Vehicle", AIAA-91-5015, AIAA 3rd International Aerospace Planes Conference, December 3-5, 1991, Orlando, FL.

[12]Gupta, K.K., Peterson, K., and Lawson, C., "On Some Recent Advances in Multidisciplinary Analysis of Hypersonic Vehicles," AIAA-92-5026, AIAA Fourth International Aerospace Planes Conference, December 1-4, 1992, Orlando FL.